AIRBORNE MEASUREMENT OF INORGANIC IONIC COMPONENTS OF FINE AEROSOL PARTICLES USING THE PILS-IC TECHNIQUE DURING ACE-ASIA AND TRACE-P

Y.-N. Lee
Atmospheric Sciences Division
Brookhaven National Laboratory
Upton, NY 11973, USA

R. Weber, Y. Ma, D. Orsini, K. Maxwell
School of Earth and Atmospheric Sciences
Georgia Institute of Technology
Atlanta, GA 30332, USA

D. Blake, S. Meinardi
University of California, Irvine, CA 92697, USA;

G. Sachse, C. Harward
NASA Langley Research Center, Hampton, VA 23681, USA

T.-Y. Chen
Institute of Geophysics
Academia Sinica
Taipei, Taiwan

D. Thornton, F.-H. Tu, A. Bandy
Department of Chemistry
Drexel University
Philadelphia, PA 19104, USA

Prepared for Journal of Geophysical Research

November 30, 2002
Revised March 6, 2003
Accepted March 11, 2003

Abstract

Eight inorganic ions in fine aerosol particles (D_p < 1.3 μm) were measured on board the NCAR C130 and NASA P-3B aircraft during the 2001 Aerosol Characterization Experiment (ACE)-Asia and the Transport and Chemical Evolution over the Pacific (TRACE-P) experiments, respectively. Concentrations of NH_4^+, SO_4^{2-}, NO_3^-, Ca^{2+}, K^+, Mg^{2+}, Na^+, and Cl^- were determined using a particle-into-liquid-sampler coupled to ion chromatography (PILS-IC) technique at a 4-min resolution and a limit of detection < 0.05 μg m^{-3}. The maximum total ion concentrations observed on the C130 and the P-3B were 27 μg m^{-3} and 84 μg m^{-3}, respectively. During ACE-Asia, NH_4^+ and SO_4^{2-} dominated, with the dust derived Ca^{2+} contributing nearly equally as SO_4^{2-} in mixing ratios. The sea-salt derived Na^+ and Cl^- were comparable to biomass burning tracer K^+, showing > 1 ppbv only in the top one percent sample population. During TRACE-P, NH_4^+ dominated, followed by SO_4^{2-}, Cl^-, Na^+, NO_3^-, Ca^{2+} and K^+, in decreasing order of importance. In addition to a sea-salt origin, Cl^- showed a source in urban emissions possibly related to biofuel combustion. Both sea-salt and dust contributed to Mg^{2+}. In both experiments, NH_4^+, SO_4^{2-}, NO_3^-, and CO were strongly correlated, indicating that combustion was the dominant source of these species and that NH_3 was in sufficient supply to neutralize SO_4^{2-}. The $[NH_4^+]$ to $([NO_3^-] + 2[SO_4^{2-}])$ ratio was ~0.70 in the two campaigns, with deviations found only in volcano plumes whereby SO_4^{2-} was found to correlate with SO_2. Charge balance of the ions showed both positive and negative deviations whose magnitudes, ~20 %, provide estimates of the lower limits of unmeasured ions. Elevated NO_3^- and Ca^{2+} coexist mainly under polluted conditions, suggesting the importance of sequestering HNO_3 by mineral dust.

1. Introduction

Atmospheric aerosol particles play many important roles in the environment, including visibility, Earth radiation budget and human health effects (NRC, 1998). In order to establish models to predict the distribution of aerosol particles (in terms of size, number and chemical composition) and to assess their environmental and health effects, knowledge of the various types of aerosol sources from different regions of the world is needed. Since many Asian countries are experiencing increased energy consumption accompanying rapid economical growth, emissions related to man-made activities are expected to rise significantly. This increased emission can impact chemical composition of the atmosphere on a regional to global scale and needs to be monitored to evaluate current effects and to predict future changes. In addition to emission sources related to man-made activities, natural sources of aerosol particles and their precursors also need to be understood. In Asia, both biomass burning and dust storms are important processes by which aerosol particles are generated.

To gain an understanding of the emission sources in Asia, two large-scale field measurement programs were carried out in 2001 to record the chemical signals of outflows from eastern and southeastern Asia. Transport and Chemical Evolution over the Pacific (TRACE-P) was an aircraft-based campaign organized by the US National Aeronautics and Space Administration (NASA). This program deployed two large research aircraft, a DC-8 and a P-3B, to measure chemical composition off the coast of China, Taiwan, Japan and Korea during the period between March 4 and April 4, 2001. Aerosol Characterization Experiment (ACE)-Asia was organized by National Science Foundation (NSF) and National Oceanographic and Atmospheric Administration (NOAA) involving ground (in Taiwan, China and Korea), shipboard (NOAA R/V Ron Brown), and aircraft (NCAR C130) measurement platforms. The C130 flew mainly

over the waters off the coast of China, Japan and Korea during the period between March 30 and May 3, 2001.

Participating in both programs, we made real-time on-line measurement of the concentrations of inorganic ionic components in fine aerosol particles (i.e., aerodynamic size diameter <1.3 μm) on board the NASA P-3B and the NCAR C130 aircraft using the recently developed particle-into-liquid-sampler coupled to ion chromatography (PILS-IC) technique (Weber et al., 2001; Lee et al., 2002; Orsini et al., 2003). NH_4^+, SO_4^{2-}, NO_3^-, Ca^{2+}, K^+, Mg^{2+}, Na^+, and Cl^- were determined at a time resolution of 4 min and a limit of detection (LOD) of 0.01~0.05 μg m^{-3}. We present in this paper a brief description of the principles and operation of the PILS-IC instrument, and an overview of the data collected on the two aircraft regarding distributions, relationships, and possible sources of these chemical components. The simultaneously measured CO, SO_2, and several hydrocarbon species which provide insights as well as constraints are used to aid the characterizations. Additional analyses of the data regarding sources, transport/mixing, and chemical processing are to be reported elsewhere (e.g., Ma et al., 2002).

2. Experimental Section

PILS-IC Instrument. The PILS-IC instruments used on board the two aircraft were identical. A detailed description of the instrument in terms of construction, operation, efficiency, size selection, and calibrations is given elsewhere (Orsini et al., 2003). Briefly, the PILS is consisted of four major components: gas denuders, a condensation particle growth chamber fitted with a steam generator, an impactor sample collector, and a dual-channel IC analysis system (Figure 1). Sample air drawn into the system (15.0 L min^{-1}) was first removed of potential gas interferents using two glass honeycomb denuders (Rupprecht & Patashnick Co., Inc. Albany, NY) placed in series immediately upstream of the condensation growth chamber. The two denuders were

coated with Na_2CO_3 and citric acid to remove acid gases (e.g., HNO_3 and SO_2) and base gases (e.g., NH_3), respectively (Sioutas et al., 1996), and were regenerated every other flight.

The sample air entering into the condensation growth chamber was mixed with steam generated from heating a 1.0 mL min^{-1} liquid H_2O flow at 110 °C, creating supersaturation conditions. Within the approximately 1 s residence time inside the chamber, particles were grown to supermicron sizes with an efficiency of ~ 90% for particle diameters of 100 nm and greater (Orsini et al., 2003). The resulting supermicron size droplets were collected using an impactor designed with a D_{50} = 1 μm (Marple and Willeke, 1976). The small liquid sample collected on the impactor surface was washed with a stream of H_2O (referred to as the carrier flow; flow rate = 0.20 mL min^{-1}) and transported to the IC system for on-line analysis.

The computer controlled IC system was comprised of one anion IC (Metrohm model 761 with a suppressor, equipped with a Metrohm Supp-5, 4 x 100 mm, anion column) and one cation IC (Metrohm model 761 without a suppressor, equipped with a Metrohm Metrosep Cation 1-2, 4 x 125 mm, column). The eluants were 4.0 mM Na_2CO_3/2.0 mM $NaHCO_3$ in H_2O for the anion IC, and 4.0 mM tartaric acid in 10% CH_3CN/H_2O for the cation IC. Both eluant flow rates were maintained at 1.0 mL min^{-1}. Since the actual sample volume (i.e., the collected droplets) varied depending on the concentration of condensable particles, the degree of dilution resulting from mixing the sample with the carrier flow also varied, albeit in a narrow range. To determine this dilution factor, a 2.0 μM $LiClO_4$ was present in the carrier flow as an internal standard. The dilution factor was determined from the actual concentration of Li^+ measured by the IC.

Inlet Systems and Particle Size Selection. The aerosol inlets on the C130 and the P-3B were different: the C130 featured a Low Turbulence Inlet (LTI) which allowed high transmission efficiencies for large size aerosol particles and the P-3B used a shrouded inlet which maintained

constant turbulence characteristics in the diffuser cone independent of the attack-angle. Because the PILS system on the P-3B was situated across the aisle from the inlet, there was an additional ~8 ft of tubing length (conductive, id = 0.75 in) between the inlet and the instrument compared to the C130 configuration. However, in spite of these differences, calculations showed that aerosol transmission efficiencies for size range 80 nm to 2.5 μm were greater than 99% in both systems.

A more restrictive size cut limitation was identified during post-experiment characterizations of the PILS system. This restriction was caused by a bend in the sample air-steam mixing region of the PILS used in the experiments and was found to effect a size cut of ~1.3 μm at the 15.0 L min^{-1} sample flow rate used (Orsini et al., 2003). As a result, the term fine aerosols used in our work has an upper size cut of 1.3 μm. Further, it was found out that the instrument's sampling efficiency for smaller particles leveled off at ~90% (Orsini et al., 2003), agreeing with filter data also collected on the P-3B for calibration purpose. The final data have been corrected for this efficiency factor.

Other Measurements. Hydrocarbons were determined by taking whole air samples in electro-polished canisters followed by laboratory GC-FID-MS analysis (Blake et al, 1997). CO was measured by a tunable diode laser absorption spectroscopy technique (Sachse et al., 1991) and SO_2 by a chemical ionization mass spectrometry technique (Thornton et al., 2002).

Flight Summary. A total of 19 research flights were performed on each aircraft. All of the 19 flights of the NCAR C130, which was stationed in Iwakuni, Japan, were made over Japan, South Korea, the Yellow Sea, East China Sea, and the Sea of Japan (between Lat 23-43 deg N and Lon 124-144 deg E , Fig. 2). In contrast, the NASA P-3B devoted 7 of its flights over the Pacific Ocean during the transit between California and Asia, leaving 12 flights covering the western Pacific region including South China Sea and the regions mentioned above. We limit

our analysis of the P-3B data to those collected in this region, i.e., Lat 7-41 deg N and Lon 112-156 deg E (Figure 2). During this western Pacific research phase, the P-3B was stationed in Hong Kong, Okinawa, and Yokota, Japan. The two aircraft missions overlapped for a 5 day period during which two intercomparison flights were conducted, one on 3/30/01 and the other 4/1/01. Concerning the PILS measurement, no data were obtained on the C130 on the 4/1/01 flight because of a logistic problem. Intercomparison of the PILS-IC data collected on the two aircraft on 3/30/01 is reported by Ma et al. (2003). The ceilings of the two aircraft were comparable: 7 km and 8 km for the P-3B and the C130, respectively. The flight durations were 8-10 hr.

3. Results and Discussion

PILS-IC data were collected on all of the 19 flights on the P-3B. For the C130 the data were missing on 3 flights: RF02 (4/1/01), RF03 (4/4/01) and RF19 (5/3/01). The total ion concentrations (the sum of the measured ions) are coded in color and displayed along the flight tracks (Fig. 2) to show the locations where elevated fine aerosol mass loading were encountered. The vertical distributions of the ions and the total ion mass concentration in three latitude bands are shown in Figure 3 and Figure 4, respectively. Because NH_4^+, NO_3^-, and SO_4^{2-} all showed much lower concentrations above 3 km, we used this altitude as an approximate division between the mixed layer and the free troposphere for displaying the probability plots of the ions (Figure 5). The maximum total ion concentration observed on the P-3B was significantly higher (84 $\mu g\ m^{-3}$) than that of the C130 (27 $\mu g\ m^{-3}$) mainly because of an encounter of a highly polluted air mass over the Yellow Sea (flight no. 14, 3/18/2001, Figure 6). Concentrations of Na^+ and Cl^- were both higher on the P-3B, but K^+ concentrations were roughly comparable. The C130

however intercepted air masses that contained much higher fine soluble Ca^{2+} than the P-3B, the maximum being 9.9 vs 4.3 $\mu g\ m^{-3}$.

Relationships between the Ions. The individual chemical species are useful tracers for identifying their sources (e.g., Andreae and Merlet, 2001). The relationship between these species, with or without a correlation, provides additional support for such analyses. Na^+ and Cl^- are thought to be primarily derived from sea-salt aerosols especially in marine environment where the ACE-Asia and TRACE-P experiments were conducted. During ACE-Asia the plot of Cl^- against Na^+ showed a slope of 1.04 with $r^2 = 0.84$ (Figure 7), fairly close to the seawater ratio of 1.16. Several data points showing high Na^+ but very low Cl^- were not used in the regression. Whether these data points are real or caused by measurement uncertainties is unknown and is being investigated. The slightly lower than sea-water ratio observed is consistent with acidification of particles by strong acids H_2SO_4 and HNO_3, resulting in a Cl^- deficit through HCl volatilization. The correlation between Cl^- and Na^+ observed on the P-3B showed a higher slope of 1.4 (Fig. 7), suggesting possible additional sources of Cl^- other than sea-salt aerosols. Since the three highest Cl^- points were found at altitude of 3-4 km and were associated with moderate Ca^{2+} concentrations, ~500 pptv, a source of Cl^- in crustal material cannot be ruled out. In addition, we also noted that Cl^- and Na^+ observed in the polluted air mass during NASA P-3B flight no.14 (Fig. 6) showed a higher ratio than those observed in cleaner air masses. While the points below the seawater ratio line (Fig. 7) may be caused by the Cl^- loss mechanism mentioned above, the points above the seawater ratio line indicate that there are additional sources of Cl^- that are associated with urban pollution which can significantly influence the Cl^-/Na^+ ratio. This observation is consistent with the report by Ye et al.(2003) that while the mean Na concentrations in Shanghai City were nearly constant over the 4 seasons (0.41-0.62 $\mu g\ m^{-3}$),

mean Cl^- concentrations increased significantly from summer (0.22 μg m^{-3}) to winter (3.54 μg m^{-3}). The fact that the samples showing elevated Cl^- are also contained high levels of K^+ (Figure 8), a biomass burning tracer (Ma et al., 2002), strongly suggests that the urban source of Cl^- is related to combustion of biofuel. This argument is also consistent with the findings of Ye el al. (2003) that both Cl^- and K^+ were elevated in Shanghai during the winter season.

Ca^{2+} is generally believed to be derived from soil and crustal material, and can therefore be used as a tracer for wind blown dusts from deserts and arid regions (e.g., Wang et al., 2002). The major forms in which calcium is found as crustal material, e.g., calcite/dolomite, are sufficiently soluble and form Ca^{2+} through hydrolysis and/or reaction with acids. Minor forms of calcium such as $Ca_3(PO_4)_2$ may not contribute to the measured Ca^{2+} because of their limited solubilities. In addition to this commonly accepted association between aerosol Ca^{2+} and its dust/crustal material origin, we are also considering the possibility that construction activities (and cement manufacturing) in major urban areas may have also played a role in aerosol Ca^{2+} content. We note that elevated Ca^{2+} concentrations were detected in the most polluted plume encountered in the TRACE-P mission (P-3B flight no. 14, Fig. 6), which has a strong urban emission characteristics judging from the high concentrations of aerosol nitrate, sulfate and many hydrocarbon species. The observed K^+ to Ca^{2+} ratio of ~3 in the first encounter of this plume (Fig. 6) is similar to the ratios (~4 in winter) of the mean concentrations of these species reported for Shanghai City (Ye et al., 2003), suggesting that an urban source of Ca^{2+} may be important and needs to be further characterized.

In the C130 data set, Mg^{2+} showed a correlation with Ca^{2+} ($r^2 = 0.83$) with a slope of 0.12, but not with Na^+ (Figure 9). However, in the P-3B data set, we noted that Mg^{2+} at elevated concentrations (> 400 pptv) were correlated with Na^+ ($r^2 = 0.78$) having a Mg^{2+} to Na^+ ratio of

0.08. This slope is fairly close to their seawater ratio of 0.11. When these high Mg^{2+} points are removed, a lower Mg^{2+} to Ca^{2+} ratio of 0.16 resulted ($r^2 = 0.69$), similar to that found on the C130. That sea-salt particles are found to contribute to Mg^{2+} observed on the P-3B is consistent with the general conditions the two aircraft platforms had experienced: the C130 saw more dust than sea-salt and the P-3B the opposite.

K^+ showed a moderate correlation with NH_4^+ and NO_3^-, r^2 being 0.47 and 0.64, respectively, during ACE-Asia, and 0.58 and 0.55 during TRACE-P. Because K^+ is thought to be associated with biomass burning (including biofuel, Ma et al., 2002), these correlations suggest that both NH_4^+ and NO_3^- have an appreciable source in these processes. It may be pointed out that the fact that elevated K^+ concentrations were observed in a highly polluted urban plume (Fig. 6) strongly supports that biofuel is an important source of this aerosol component. Ye et al (2003) showed that K^+ was important in Shanghai and that the mean concentration increased by ~3 fold from summer (0.89 $\mu g\ m^{-3}$) to winter (3.2 $\mu g\ m^{-3}$), corroborating the elevated K^+ we measured.

NH_4^+ was strongly correlated with NO_3^- and SO_4^{2-} (r^2 being 0.66 and 0.69, respectively, during both ACE-Asia and TRACE-P), and stronger still with the sum of NO_3^- and SO_4^{2-} (Figure 10), suggesting that NH_3 shared common emission sources with NO_3^- and SO_4^{2-} and their precursors. One may note that NH_3 is emitted at a significant level (~1% of CO) from vehicles equipped with the modern 3-way catalytic converters (Perrino et al., 2002). If a slope of unity was observed in these plots (Fig. 10), then a complete neutralization by NH_3 of HNO_3 and H_2SO_4 is indicated. However, since the best fit slope was 0.68, it indicates that on average there is a ~30% of deficit in NH_4^+ compared to NO_3^- and SO_4^{2-}. This deficit is therefore made up by other unmeasured cations, including organic species (e.g., amines), soil derived species (e.g., Fe and

Mn) and the hydronium ion (acid aerosols). However, since H_2SO_4 is a much stronger acid than HNO_3 and exhibits a negligible vapor pressure compared to HNO_3, aerosol NO_3^- resulting from condensation of gas phase HNO_3 with available NH_3 (or other alkaline reagents) will become important only after H_2SO_4 is fully neutralized (Seinfeld and Pandis, 1997). Consequently, the presence of NO_3^- in aerosols can be taken to indicate that the aerosol particles are no longer acidic and to assess the relative source strengths of NH_3 and the total sulfur (dominated by SO_2 at emission sources). From the fact that > 90% of the samples collected below 3 km, i.e., 1133 out of the 1161 collected on the C130 and 729 out of the 812 on the P-3B, contained non-zero NO_3^- (i.e., $[NO_3^-]/[SO_4^{2-}] > 0.02$), we conclude that under most conditions NH_3 and other alkaline materials, e.g., amines, were emitted in quantities comparable or greater than H_SSO_4 and its precursor SO_2.

The altitude dependence of the ratio of NH_4^+ to the sum of NO_3^- and SO_4^{2-} is shown in Figure 11. The locally weighted regression scatterplot smoothing (Lowess) shown as the solid line, which approximates the median, indicates for the C130 data a slight negative departure from the best fit slope of 0.68 in the 3 to 6 km range and a positive departure above 6 km. For the P-3B data, the ratio decreased from ~0.8 at lower altitudes to ~0.5 at higher altitudes. In both experiments, this ratio remained fairly constant below 3 km and showed departures only above this altitude. This behavior agrees with the 3 km height used to divide the mixed layer and the free troposphere (Fig. 5) for which air masses of different sources and history are expected to be encountered. We used the Lowess fit because it was more convenient than the common practice of showing box plots of binned data.

The co-emission of NH_3 along with aerosol sulfate and its precursor SO_2 is also observed during a study of the plume of the Miyakejima volcano (24.08N, 139.53E, P-3B flight no.17,

3/27/2001). Sampling was carried out approximately 200 to 300 km downwind of the volcano to the east southeast of the volcano. The molar ratio of $[NH_4^+]$ to $2[SO_4^{2-}]$ decreased with increasing aerosol SO_4^{2-}, reaching an asymptotic value of 0.42 ± 0.016 (Fig. 12). Because the analysis was confined to samples associated with the volcanic plume (altitude < 2km; $[SO_2] > 2$ ppbv), the reaching of an NH_4^+ to SO_4^{2-} equivalent ratio at 0.42 indicates that NH_3 was released at a molar ratio roughly similar to that of SO_2. Because we expect a titration behavior in the $[NH_4^+]/[SO_4^{2-}]$ ratio if NH_3 is the only neutralizing reagent, the fact that the ratio reached an asymptotic value of 0.42 without showing an end point strongly suggests the presence of other alkaline materials. We speculate that amines were among the candidates. It is noted that SO_4^{2-} was correlated with SO_2 (Figure 13) suggesting that the oxidation of SO_2 to H_2SO_4 is the rate limiting step of aerosol SO_4^{2-} production.

Charge Balance. Charge balance of the observed aerosol ionic components offers insights into whether the major ionic species comprising the aerosol particles have been identified and quantified. Further, in the case of departure from neutrality, we may estimate the possible identities of the missing ionic species and their contributions. In addition, measurement reliability can also be evaluated through this examination.

In Figure 14 we plot the total positive charges against the total negative charges (in pptv-equivalent) found in the samples. For the C130, the best fit shows a slope of 0.91 and a large intercept of 648 pptv-eq. The correlation coefficient of this scatter plot is 0.67, reflecting the fairly sizable scatter of the data. However, we note that all the points lie above the 1:1 ratio line contained elevated levels of Ca^{2+}, i.e., $[Ca^{2+}] > 1.0\ \mu g\ m^{-3}$. A plausible explanation of this observation is that the anions associated with Ca^{2+} were not completely identified by our

measurement technique. A possible candidate of this missing anion is CO_3^{2-}, which is known to be associated with crustal material derived Ca^{2+} and was not quantified by our IC technique.

To examine whether all of the anions associated with Ca^{2+} were undetected and therefore resulted in the large positive deviations seen in Figure 14, we plot the same data but with Ca^{2+} removed from the total positive charge (Fig. 14). While the correlation coefficient increased to 0.80, the best fit slope only slightly lowered to 0.82, with large scatters evenly distributed about the 1:1 line. This indicates that Ca^{2+} rich samples with potentially unquantified anions contributed only a portion of the positive deviation in the charge balance. It was noted that neither Cl^- nor SO_2 caused a bias in the observed scatter; data points with high values of these two species were roughly evenly distributed about the 1:1 ratio line. With the aerosol chemical composition knowledge already established (e.g., Seinfeld and Pandis, 1997), we recognize that organic compounds are also important components of aerosols. Excess negative charges reflect the presence of unmeasured cations, including metals, amines and strong acids. Excess positive charges, on the other hand, indicate unmeasured anions such as carboxylates (Kawamura, 1999). However, because NO_3^- was present in most of the samples as pointed out earlier, acid aerosols can only account for an upper limit of 10%. The red data points (Fig. 14) exhibiting the largest negative deviations are those identified in Figure 10 having the lowest ratio of NH_4^+ to ($NO_3^- + SO_4^{2-}$), suggesting that in these cases the strong acid, H_2SO_4, might not be fully neutralized and were responsible for the observed negative deviation.

The plots of total positive to negative charges are given in Figure 15 for the P-3B data. As with the C130 data, samples containing higher Ca^{2+} tended to lie above the 1:1 line. The best fit slope, 0.83, is similar to that of the C130 data with Ca^{2+} removed. However, we note that samples corresponding to high SO_2 concentrations were responsible for a low positive to

negative charge ratio. The red points in Figure 15 with SO_2 in excess of 10 ppbv were identified to be those collected in the Miyakejima volcano plumes during P-3B flight no. 17. It is interesting to point out that most of the high SO_2 points not associated with the volcanic plumes showed a charge balance very close to unity, again supporting the notion that alkaline materials, principally NH_3, is co-emitted at a level similar to or greater than the acid aerosols and their precursors. There are fewer data points in this figure because SO_2 was not determined on all the P-3B flights.

The magnitude of the charge imbalance, i.e., total positive charges minus total negative charges, is plotted in Figure 16 as a function of the total concentration of the ions. Since we did not include Ca^{2+} in this plot, the magnitude of positive deviations indicated in Fig.16 represent a lower limit as some of the anions associated with Ca^{2+} such as SO_4^{2-} which are not removed along with Ca^{2+} would give rise to a negative bias to this ion imbalance. The Lowess fit of the negative deviations showed a "median" of -60% at the lowest total ion concentration which then decreased to -18 % at 3 ppbv and remained at that level for the higher concentration regime. The Lowess fit of the positive deviations reduced from 37% at the lowest concentrations to 24% at 3 ppbv, and then remained between 20 to 15% in the higher concentration range. The P-3B data showed a similar magnitude of percent deviation from a complete charge balance but slightly more negative within the concentration range of the C130 (maximum = 14 ppbv).

Since the limit of detection of the PILS-IC were 10 ng m^{-3} and 50 ng m^{-3} for the anions and cations, respectively (Orsini et al., 2003), we estimated a measurement uncertainty in the total anion to be ~10 pptv and total cations to be ~110 pptv. The total uncertainty in the ion imbalance calculation is ~110 pptv, being dominated by the cations' uncertainty. It is clear that this small measurement uncertainty contributed negligibly to the observed scatter in Fig. 16,

accounting for only 10% at a total concentration as low as 1 ppbv. One notes that the higher LOD for cations may be responsible for a larger negative deviation in charge balance at the lowest aerosol mass loading because values below LOD were assigned as zero.

It is noted that one should not consider only those samples exhibiting charge imbalance to have unidentified organic ions. Since neither organic ions nor the strong acid, hydronium ion, were measured, it is unlikely that we can rule out the presence of these components for samples that did show a reasonable charge balance. Two corollaries that follow are: (1) no a priori expectation of a normally distributed charge balance centered at zero based on the 8 measured ions, and (2) the missing charges can only be used to arrive at lower limit estimates for the concentrations of unmeasured ionic species.

Altitude Dependence of Charge Imbalance. We plot the charge imbalance (with and without Ca^{2+}) as a function of altitude in Figure 17 to inspect whether the imbalance exhibits any altitude dependence. The Lowess fits of the C130 data show that the surrogate median value is very near zero at the lowest altitude, and increases with increasing altitude reaching +60% at the maximum altitude of 8 km. With Ca^{2+} ion removed, the median remains at ~zero from the lowest altitude to 5 km and then increases to +30% at the highest altitude. The data points with total ion concentration less than 500 pptv which are expected to show the largest percent measurement uncertainties ($\geq$ 20%, Fig.17) did not show a significantly different pattern in either magnitude or sign of the departure from the remaining data, indicating that measurement uncertainties contributed insignificantly to the observed charge imbalance. The P-3B data which included the Ca^{2+} showed an increase in positive deviation with increasing altitude, similar to the C130 data. The lower concentration data points (total ion < 500 pptv) appeared to exhibit a

wider spread in the imbalance, suggesting that measurement uncertainties were partly responsible for the observed charge imbalance.

Relationships of Aerosol Ionic Components with other Measurements. Fine aerosol particles are known to have an important source in combustion processes which produce precursors such as SO_2, hydrocarbons, and NO_x in addition to primary particulate matter such as soot containing particles. Since CO is a major byproduct of combustion, a correlation between CO and fine aerosol mass loading (and some aerosol chemical components) is expected. In Figure 18 we plot the sum of the concentrations of NH_4^+, SO_4^{2-}, NO_3^-, and K^+ against CO. Na^+, Cl^-, Ca^{2+}, and Mg^{2+} were not included because they are considered non-combustion related. Although the majority of the C130 data points conform to a fairly strong correlation (Fig. 18), there is a separate group of samples that showed much smaller ratios, i.e., [CO] ranging between 230 and 1000 ppbv with corresponding [total ion] between 0 and 1 ppbv. Since these data points also correspond to similarly low ratios of other species to CO, e.g., toluene and ethane, we surmise that these data points were collected in air masses that had been substantially processed, e.g., by photo chemical reactions, leaving, however, the long lived CO relatively unchanged.

To investigate this possibility, we establish a time scale that can approximate the photochemical age of an air mass using the measured hydrocarbon concentrations. Ratios of co-emitted hydrocarbons, e.g., benzene and toluene from automobile exhausts, have been applied to determining the plume age (Gelencser et al., 1997). While this approach has the advantage of being insensitive to dilution, good knowledge of the ratios of the hydrocarbons at the source is required. Further, a realistic average OH concentration is also needed. Since fairly large uncertainties exist in both quantities, the photochemical age estimated here is at best qualitative.

However, somewhat favorable for the ACE-Asia and TRACE-P environment is that there are fewer nearby sources over the ocean that can confound this ratio.

From the selected hydrocarbon species available we used ethyne and toluene for this calculation because both are known to have a strong source in vehicular emissions. Using a source ethyne/toluene ratio of 0.65 (Fraser et al., 1998) and a 24-hr average [OH] of 5.5×10^6 cm^{-3}, we derived a photochemical age ranging from 8 hr to 51 hr (C130). This time scale agreed with that established using propane and toluene to within 10 hrs. Although the C130 data in Fig. 18 showing a small ion mass to CO ratio were somewhat aged, 30 to 51 hr, there are significantly more data points in this age group belonging to the higher slope group of Fig. 18. Consequently, it is clear that photochemical reactions (within ~2 days) were not the primary process by which aerosols were removed from the atmosphere. Cloud processing which preferentially removes soluble species is likely to be responsible for the low [Ions] to [CO] ratios in these samples. Since cloud processing is often accompanied by rise of air masses to higher altitudes, samples collected at higher altitudes may have increased chance of going through such a process. In this regard, we note that 31 of the 34 samples in this group were collected at altitude greater than 2 km. Least squares best fits are determined for the two different groups (Fig. 18).

We noted that the inclusion of the non-combustion related ions did not affect the correlation, with the r^2 remaining at 0.82. This is not unexpected concerning Na^+ and Cl^- as their concentrations were low. However, this also indicates that Ca^{2+} which was present at much higher concentrations had been relatively well mixed with combustion plumes. Furthermore, it's worthwhile noting that in Fig. 18 samples containing elevated K^+ are associated with the high [CO]. Since K^+ is believed to be a tracer for biomass (and biofuel) burning, the inefficient

combustion process which is known to generate a significant amount of CO is corroborated by this observation.

A brief diversion follows. It should be cautioned that the qualitative photochemical age analysis carried out here is based on the assumption that vehicular-derived urban pollution in large Chinese cities (e.g., Shanghai) is similar in character to that of the U.S. However, the validity of this assumption may be partly supported by two considerations. First, China has a policy in place keeping vehicles older than 10 years off the road and as a result the fleet is dominated by modern vehicles, most of them produced in China by major international nameplates. Second, despite the fact that the air sampled on the P-3B were impacted by various regions, including Hong Kong, Japan, Korea and China, tight correlation between several key hydrocarbon species (e.g., toluene, benzene, i-pentane, n-butane) were observed on the P-3B similar to those observed in North America (e.g., Parrish et al., 1998),

A similar analysis is made for the P-3B data in Figure 18. Although K^+ is again found to be associated with high [CO], the data did not form a clearly distinguishable groups like the C130 data. We nonetheless fitted the data without the group which showed [Ion] less than 1 ppbv and [CO] greater than 250 ppbv. The slope of the best fit line is nearly twice as that for the C130 data, resulting from less aged high concentrations of pollution encountered by the P-3B. It may be pointed out that the photochemical age of the most polluted urban plume encountered (the first plume in Fig. 8) was estimated to be ~20 hr using the benzene/toluene pair. These low ion-high CO samples were found to have elevated CH_3Cl (600-1000 pptv), but contained essentially zero K^+, consistent with cloud processing which had preferentially removed the soluble species. The altitude at which these points were sampled ranged between 0.6 and 6 km with 49 out of 72 above 2 km. The eyeballed maximum slopes using the top of the data envelops

are not too different between the C130 and the P-3B, providing a qualitative estimate for the ion (including precursors) to CO emission ratio of 5%.

Relationship between Ca^{2+} and NO_3^-. Ca^{2+} (and other mineral cations) contained in dust aerosols serves as an important neutralizing and quenching reagent for acids produced in the gas phase (e.g., nitric and sulfuric acids). Although it has been suggested that mineral particle can also mediate chemical transformation (Dentener et al., 1996) by way of surface reaction oxidizing NO_2 to NO_3^-, field observations needed to support this mechanism have not been unequivocally established. A major difficulty in verifying this pathway lies in the fact that gas phase formation of HNO_3 from NO_2 oxidation by OH followed by adsorption onto mineral particles is typically fast, characteristic NO_2 life time being < 24 hr. The data collected on the C130 and P-3B again showed that samples of high aerosol NO_3^- are associated with high CO where active photochemical production of HNO_3 is expected. In Figure 19 we plot the percent positive charge due to Ca^{2+} as a function of aerosol $[NO_3^-]$. While it is clear that Ca^{2+} played an important role as a neutralizing reagent, accounting for ~50% of the positive charges at $[NO_3^-]$~ 1.5 ppbv, elevated $[NO_3^-]$, i.e., greater than 200 pptv, were nearly exclusively associated with $[CO] \geq 200$ ppbv. Only the C130 data were shown because of the larger Ca^{2+} concentration observed on this platform.

4. Conclusions

Fine aerosol ionic components, NH_4^+, SO_4^{2-}, NO_3^-, K^+, Ca^{2+}, Mg^{2+}, Na^+, and Cl^-, were determined at a 4-min time resolution using a PILS-IC technique on board the NCAR C130 and NASA P-3B during the ACE-Asia and TRACE-P experiment, respectively. The maximum total ion concentration observed on the P-3B was 84 $\mu g\ m^{-3}$, significantly higher than that on C130, 27 $\mu g\ m^{-3}$, because of an encounter of highly polluted air mass over the Yellow Sea. The timing and

location, however, allowed the C130 to sample air masses that were heavily impacted by dust particles indicated by the elevated Ca^{2+} concentrations (maximum = 6 ppbv). Low levels of Mg^{2+} were also derived from dust at a Mg/Ca ratio of ~ 0.16. Higher levels of Mg were found to have a sea-salt origin showing a Mg/Na ratio of ~0.1. Cl^- and Na^+ were in general correlated, the slope being close to their seawater ratio. However, additional sources of Cl^- in urban emissions and dust plumes were also indicated. SO_4^{2-}, NO_3^-, and K^+ all showed strong correlations with CO, consistent with their combustion origins. NH_3, which appeared to also be co-emitted from the combustion processes and urban areas, was comparable in supply to H_2SO_4 and its precursor SO2, responsible for neutralizing ~70% of the total aerosol acidity. Charge balance of the 8 measured ions showed that although the positive and negative charges are tightly correlated, slope ≥ 0.8, the magnitude of the imbalance (positive charge-minus charge, in pptv-eq) was ≥ 20% of the total ion concentration (in pptv). It is expected that these missing charges are associated with organic acids and bases in addition to the hydronium ion. The unmeasured chemical components were likely to also be present even in cases where an apparent charge balance was observed. The charge imbalance did not show an altitude dependence and was not significantly influenced by measurement uncertainties.

Acknowledgements

This research was supported by NSF and NOAA Office of Global Change Program for the ACE-Asia Project and by NASA GTE for the TRACE-P Project. The participation of YNL in the ACE-Asia and TRACE-P was supported by NOAA through an interagency agreement and by NASA through a subcontract with Georgia Institute of Technology, respectively. We thank Dr. T. Anderson of U. of Washington for helpful comments and suggestions.

References

Andreae, M. O. and P. Merlet. Emission of trace gases and aerosols from biomass burning. Global Biogeochemical Cycles, 15, 955-966, 2001.

Blake, D. J., D. R. Blake, T.-Y. Chen, J. E. Collins, Jr., G. W. Sachse, B. E. Anderson, and F. S. Rowland. Distribution and seasonality of selected hydrocarbons and halocarbons over the western Pacific basin during PEM-West A and PEM-West B. J. Geophys. Res., 102, 28315-28331, 1997.

Dentner, F. J., G. R. Carmichael, Y. Zhang, J. Lelieveld, and P. Crutzen. Role of mineral aerosol as a reactive surface in the global troposphere. J. Geophys. Res., 101, 22869-22889, 1996.

Fraser, M. P., G. R. Cass, and B. R. T. Simoneit. Gas-phase and particle-phase organic compounds emitted from motor vehicle traffic in a Los Angeles roadway tunnel. Environ. Sci. Technol., 32, 2051-2060, 1998.

Gelencser, A., K. Siszler, J. Jlavay. Toluene-benzene concentration ratio as a tool for characterizing the distance from vehicular emission sources. Environ. Sci. Technol., 31, 2869-2872, 1997.

Kawamura, K. and F. Sakaguchi. Molecular distributions of water soluble dicarboxylic acids in marine aerosols over the Pacific Ocean including tropics. J. Geophys. Res., 104, 3501-3509, 1999.

Lee, Y.-N., Z. Song, Y. Liu, P. Daum, R. Weber, D. Orsini, N. Laulainen, J. Hubbe, V. Morris. Aerosol chemical characterization on board the doe g1 aircraft using a particle-into-liquid-sampler during the TexAQS 2000 experiment. Extended Abstract published at the 82nd Annual AMS Meeting, Orlando, FL, January 13-17, 2002. Paper no. 10-13.

Ma et al., The characteristics and influence of biomass burning aerosols on fine particle ionic composition measured in Asian outflow during TRACE-P. J. Geophys. Res., TRACE-P special issue, 2002. Submitted.

Ma et al., Intercomparison of airborne measurements of aerosol ionic chemical composition during TRACE-P and ACE-Asia. J. Geophys. Res., 2003. Manuscript in preparation.

Marple, V.A., and K. Willeke. Impactor design. Atmos. Environ., 10, 891-896, 1976.

NRC. Research priorities for airborne particulate matter: I. Immediate priorities and a long-range research portfolio. Committee on research priorities for airborne particulate matter, National Research Council, Washington, DC, 1998.

Orsini, D. A., Y. Ma, A. Sullivan, B. Sierau, K. Baumann and R. J. Weber. Refinements to the particle-into-liquid sampler (pils) for ground and airborne measurements of water soluble aerosol composition. Atmos. Environ., 2003. In Press.

Parrish et al., Internal consistency tests for evaluation of measurements of anthropogenic hydrocarbons in the troposphere. J. Geophys. Res., 103, 22339-22359, 1998.

Perrino, C., M. Catrambone, A. Di Menno Di Bucchianico, and I. Allegrini. Gaseous ammonia in the urban area of Rome, Italy and its relationship with traffic emission. Atmos. Environ., 36, 5385-5394, 2002.

Rogge, W. F., M. A. Mazurek, L. M. Hildemann, G. R. Cass, and B. R. T. Simoneit. Quantification of urban organic aerosols at a molecular level: identification, abundance and seasonal variation. Atmos. Environ., 27A, 1309-1330, 1993.

Sachse, G. W., J. E. Collins, Jr., G. F. Hill, L. O. Wade, L. G. Burney, and J. A. Ritter. Airborne tunable diode laser system for high precision concentration and flux

measurements of carbon monoxide and methane. Proc. SPIC int. Opt. Eng., 1433, 145-156, 1991.

Seinfeld J. H. and S. N. Pandis. "Atmospheric Chemistry and Physics: From Air Pollution to Climate Change", J. Wiley, New York, 1997.

Sioutas, C., P. Y. Wang, S. T. Ferguson, P. Koutrakis, and J. D. Mulik. Laboratory and field evaluation of an improved glass honeycomb denuder/filter pack sampler. Atmos. Environ., 30, 885-895, 1996.

Thornton, D. C., A. R. Bandy, F. H. Tu, B. W. Blomquist, G. M. Mitchell, W. Nadler, and D. H. Lenschow. Fast airborne sulfur dioxide measurement by atmospheric pressure ionization mass spectrometry (APIMS). J. Geophys. Res., 2002. TRACE-P special issue. Submitted.

Wang, Z., H. Akimoto, and I. Uno. Neutralization of soil aerosol and its impact on the distribution of acid rain over east Asis: observations and model results. J. Geophys. Res., 107, ACH-X, doi: 10.1029/2001JD001040, 2002.

Weber, R. J., D. A. Orsini, Y. Duan, Y. -N. Lee, P. J. Klotz, and F. Brechtel. A particle-into-liquid collector for rapid measurement of aerosol bulk chemical composition. Aerosol Sci. Technol. 35, 718-727, 2001.

Ye, B., X. Ji, H. Yang, X.Yao, C. K. Chan, S. H. Cadle, T. Chan, and P. A. Mulawa. Concentration and chemical composition of PM2.5 in Shanghai for a 1-year period. Atmos. Environ., 37, 499-510, 2003.

Figure Captions.

Figure 1. Schematic diagram of the PILS-IC instrument deployed on the NCAR C130 and NASA P-3B. Sample flow rate was 15 L min^{-1} during TRACE-P and ACE-Asia.

Figure 2. Flight tracks of the NCAR C130 and NASA P3-B during ACE-Asia and TRACE-P, respectively. The total measured ion concentrations are color-coded according to the color bars (the maximum concentrations are beyond that indicated by the color bars); large size symbols denote altitudes below 3 km, narrow lines above 3 km, and intermediate size between 2.7 and 3 km. The total numbers of PILS-IC samples are indicated.

Figure 3. Vertical distributions of SO_4^{2-} ;NH_4^+, NO_3^-; Ca^{2+}, K^+; and Na^+, Cl^- in three latitude bands (deg N): >30, 30 < Lat < 35, and >35.

Figure 4. Vertical distribution of total ion mass concentration grouped by latitude. The black lines represent locally weighted average.

Figure 5. Frequency distributions of aerosol ionic components in two different altitude ranges, below and above 3 km

Figure 6. Time series of the concentrations of several aerosol ionic components observed during NASA P-3B flight no. 14 (3/18/2001) where a most polluted air mass during the entire mission was encountered.

Figure 7. Correlation between aerosol Cl^- and Na^+. The solid lines represent the least squares fits. Data points in the rectangular box were not used in the regression.

Figure 8. Scatter plot of Cl^- vs Na^+ observed on NASA P-3B flight no. 14. The dashed line represents the sea water ratio of these two species (slope = 1.16). Data points are color-coded according to K^+ concentration.

Figure 9. Correlation between Mg^{2+} and Ca^{2+}.

Figure 10. Correlation between NH_4^+ and the sum of NO_3^- and SO_4^{2-}. The solid line represents the best fit with data points (in red) showing a significant departure from the main group removed ($r^2 = 0.95$).

Figure 11. Altitude dependence of the ratio of NH_4^+ to the sum of NO_3^- and SO_4^{2-}. The solid curve represents the Lowess average, which approximates the median values. The dotted line is the slope of the best fit in the previous figure. Seventeen points with $[NH_4^+]/([NO_3^-]+2[SO_4^{2-}]$ ratio greater than 5, mostly in the altitude range 5 to 7 km, are not shown.

Figure 12. Ratio of $[NH_4^+]$ to $2[SO_4^{2-}]$ as a function of aerosol sulfate concentration observed during a volcano plume study (NASA P-3B flight no. 17, 3/27/2001). Data are color coded to SO_2 concentration and size coded to altitude (less than 2 km if larger than the smallest point in the graph). The exponential fit of the data is limited to those associated with the Miyakejima volcanic plume using $[SO_2] > 2$ ppbv as a criterion. (SO_2 maximum was 17 ppbv, but clipped at 10 ppbv in the color scale for a better low range resolution.)

Figure 13. Relationship between aerosol SO_4^{2-} and SO_2 in the volcanic plume of Miyakejima. The solid line represents the best fit of the data for $SO_2 > 2$ppbv ($r^2 = 0.80$).

Figure 14. Charge balance of the measured aerosol ionic components during ACE-Asia. Top plot: color-coded to Ca concentration; the solid blue line is the least-square fit of data

points. Bottom plot: without Ca^{2+}; the red data points are those identified in Figure 10 as having large $(NO_3^- + SO_4^{2-})/NH_4^+$ ratios..

Figure 15 . Charge balance of measured ions on the NASA P-3B during TRACE-P. Top plot: Color coded to Ca^{2+} concentration. Bottom plot: color coded to SO_2 concentration; the two lines are the same as those in the top graph.

Figure 16. Charge imbalance of the measured aerosol ionic components as a function of total ion concentration. The solid line represents the best fit of the data and the upper panel shows the deviation of the imbalance from zero normalized to total ion concentration.

Figure 17. Ion imbalance as a function of altitude observed on the NCAR C130 (top) and on the NASA P-3B (bottom). Points with a total ion concentration less than 500 pptv are shown in solid circles. The solid lines represent Lowess fits to the data.

Figure 18. Correlation between the sum of ions (NO_3^-, SO_4^{2-}, NH_4^+, and K^+) and CO. Top: The group of points showing distinctly low ratios are treated separately; r^2 are 0.82 and 0.54, respectively. The dashed line is the eyeballed top edge of the data envelope. Bottom: The solid line is the best fit of the data without the group with [Ion] < 1 ppbv and [CO] > 250 ppbv. The dashed line is again the eyeballed top of the data envelop and the dotted line is the best fit line of the NCAR C130 data.

Figure 19. Contribution of Ca^{2+} to positive charges as a function of aerosol nitrate concentration.

Figure 1. Schematic diagram of the PILS-IC instrument deployed on the NCAR C130 and NASA P-3B. Sample flow rate was 15 L min^{-1} during TRACE-P and ACE-Asia.

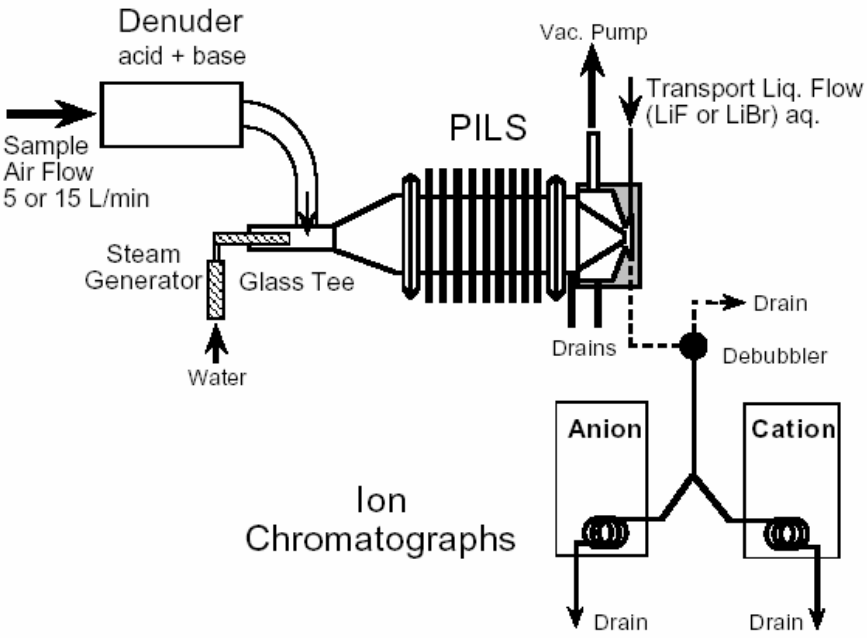

Figure 2. Flight tracks of the NCAR C130 and NASA P3-B during ACE-Asia and TRACE-P, respectively. The total measured ion concentrations are color-coded according to the color bars (the maximum concentrations are beyond that indicated by the color bars); large size symbols denote altitudes below 3 km, narrow lines above 3 km, and intermediate size between 2.7 and 3 km. The total numbers of PILS-IC samples are indicated.

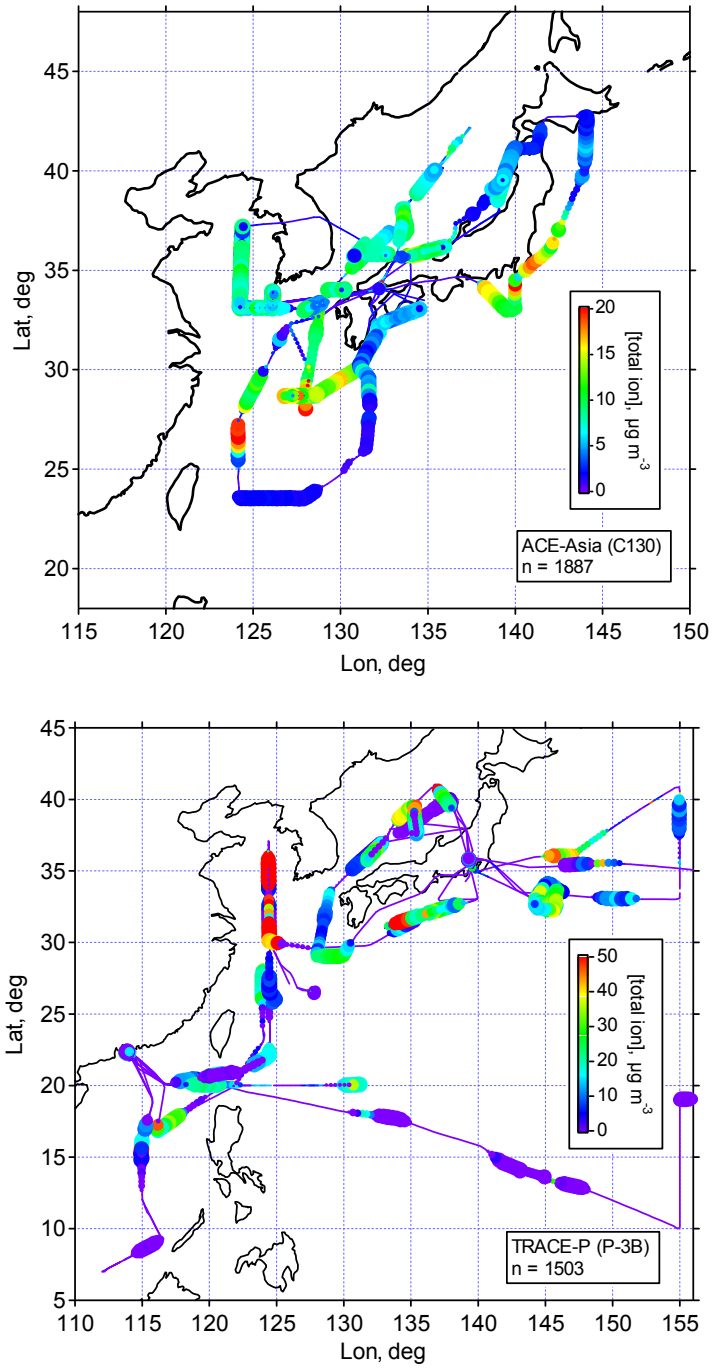

Figure 3. Vertical distributions of SO_4^{2-} ;NH_4^+, NO_3^-; Ca^{2+}, K^+; and Na^+, Cl^- in three latitude bands (deg N): >30, 30 < Lat < 35, and >35.

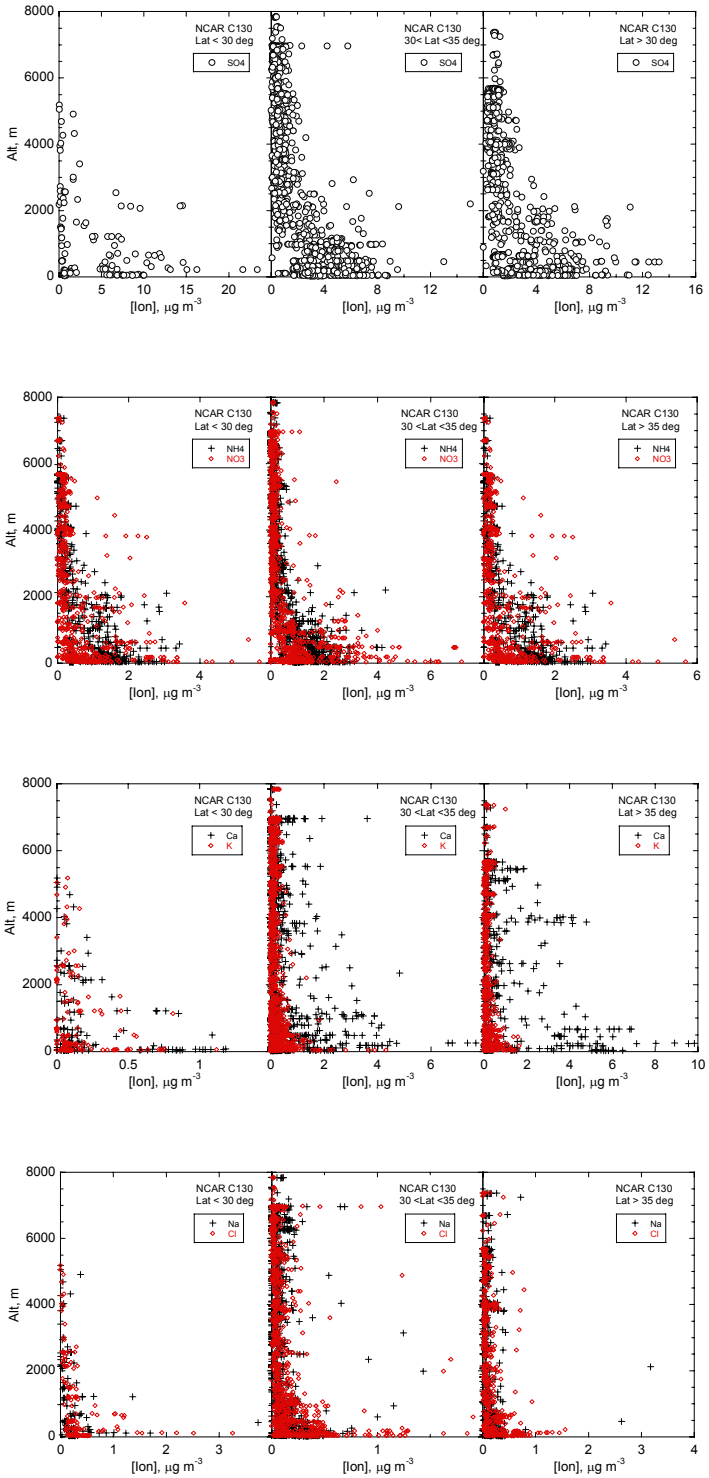

Figure 3. Continued

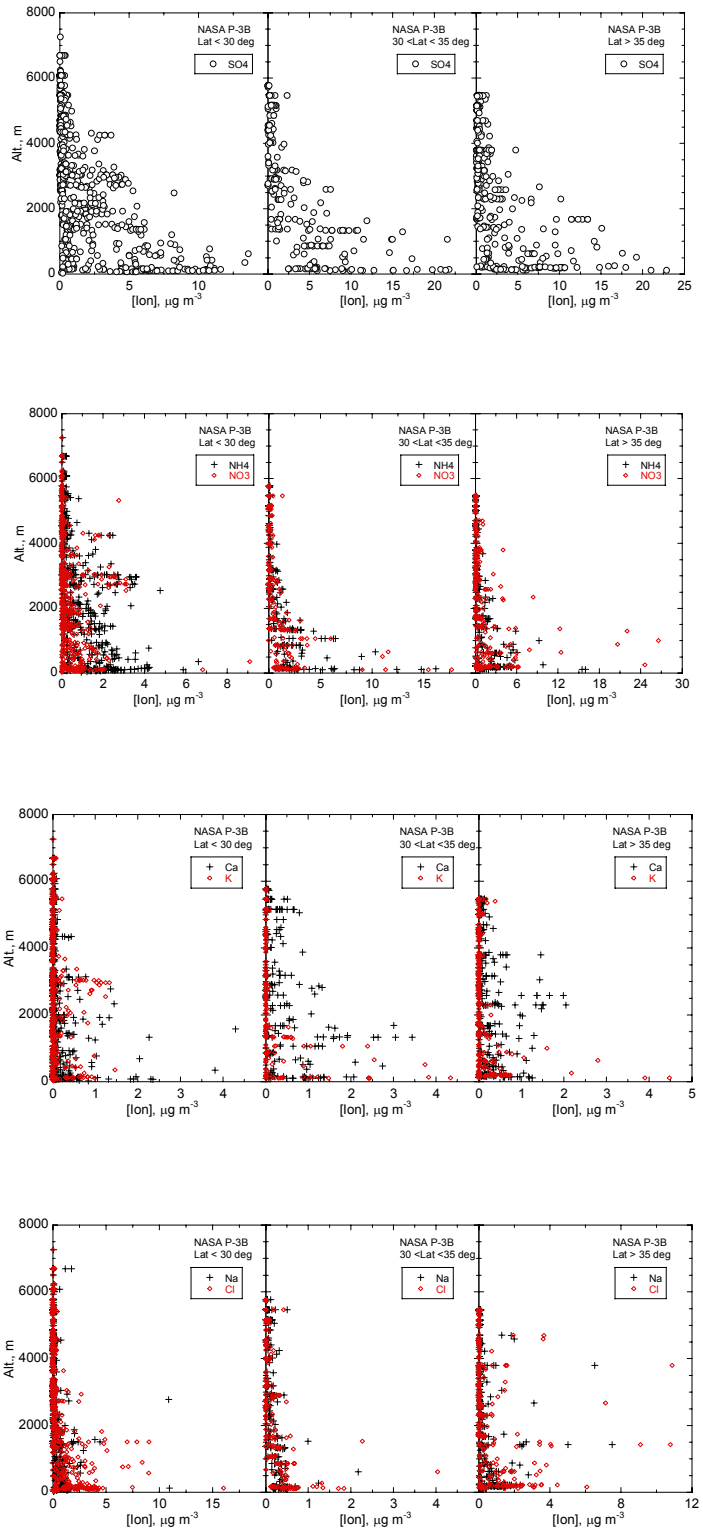

Figure 4. Vertical distribution of total ion mass concentration grouped by latitude. The black lines represent locally weighted average.

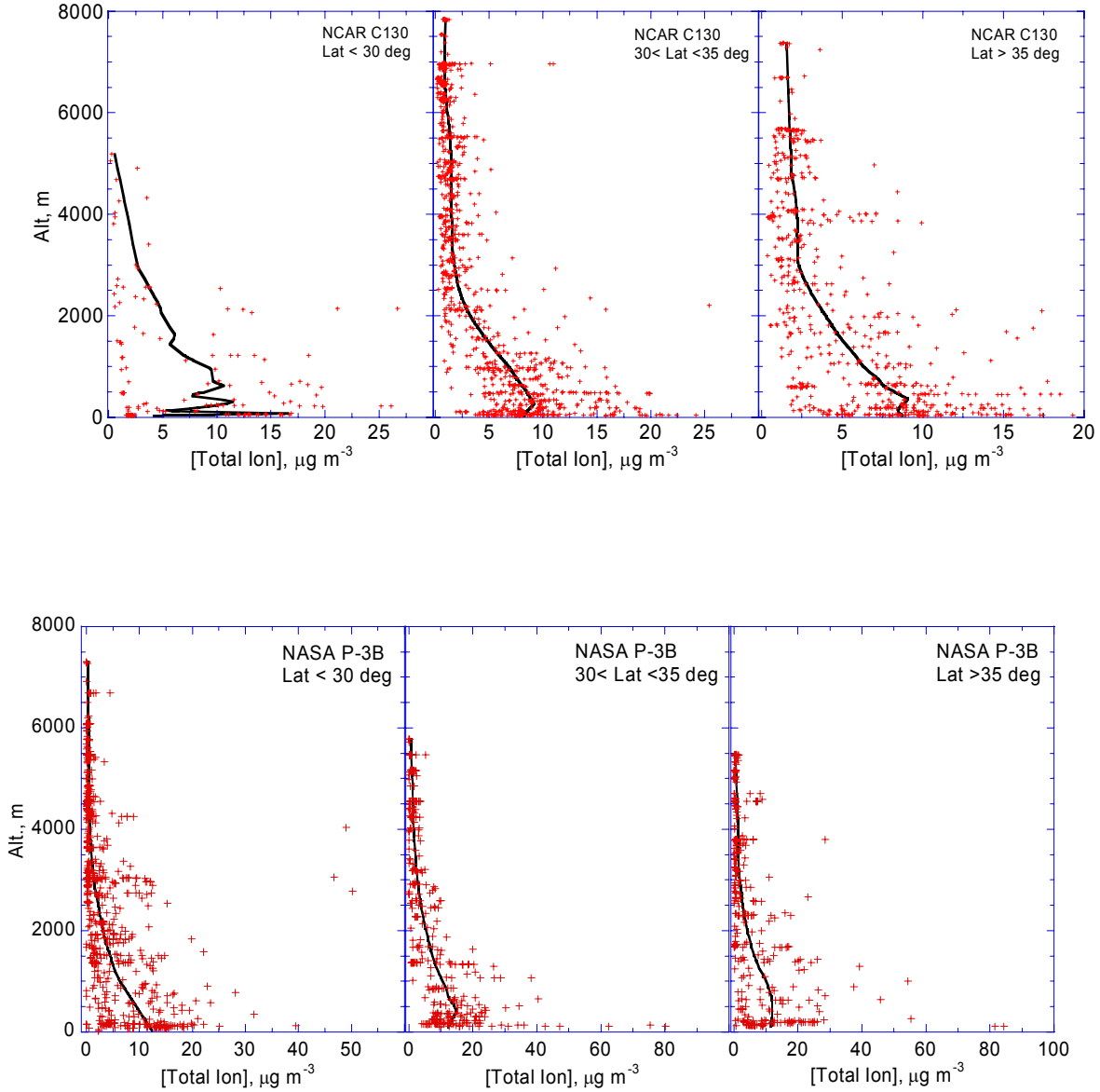

Figure 5. Frequency distributions of aerosol ionic components in two different altitude ranges, below and above 3 km.

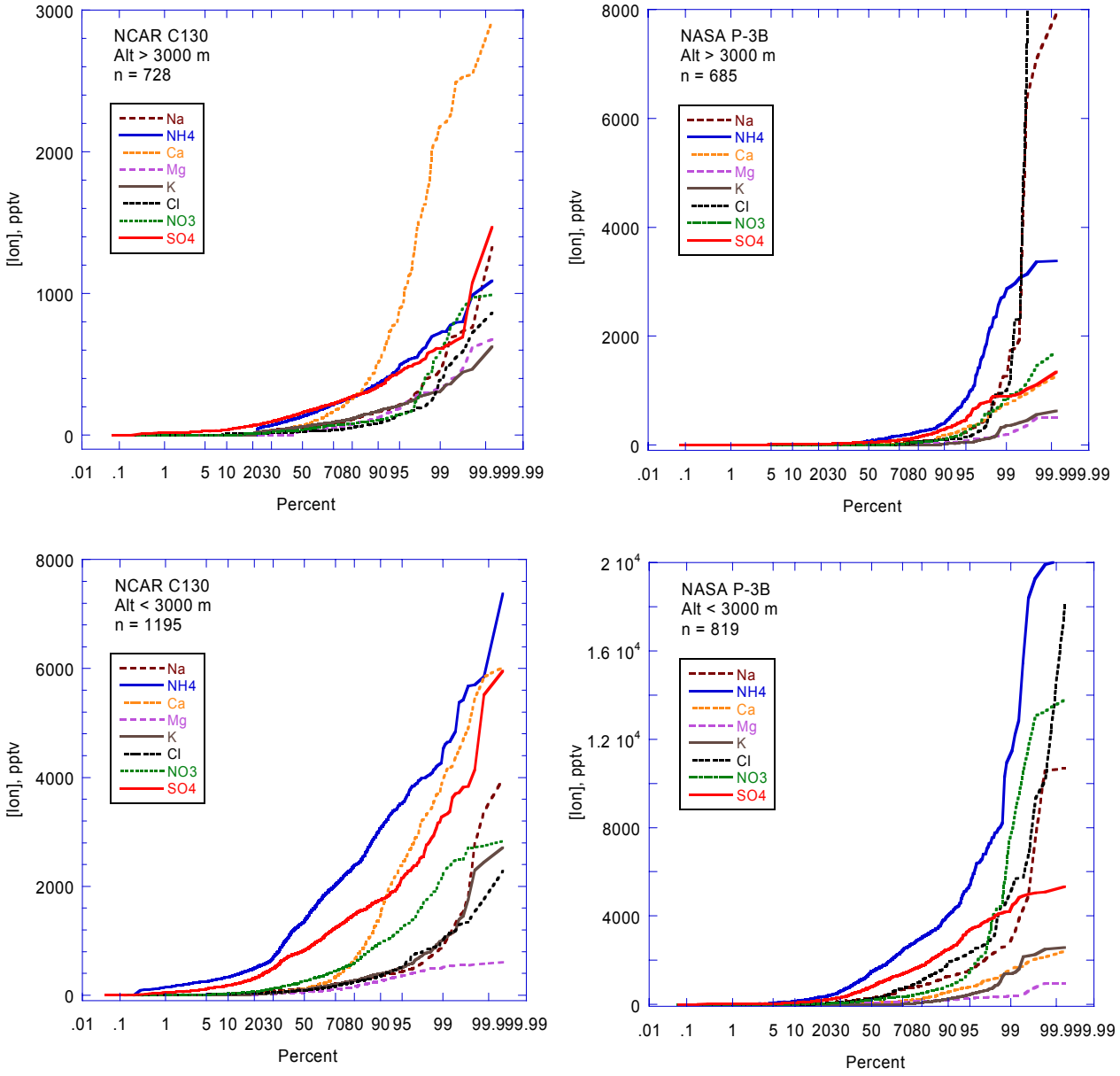

Figure 6. Time series of the concentrations of several aerosol ionic components observed during TRACE-P flight no. 14 where a most polluted air mass during the entire mission was encountered.

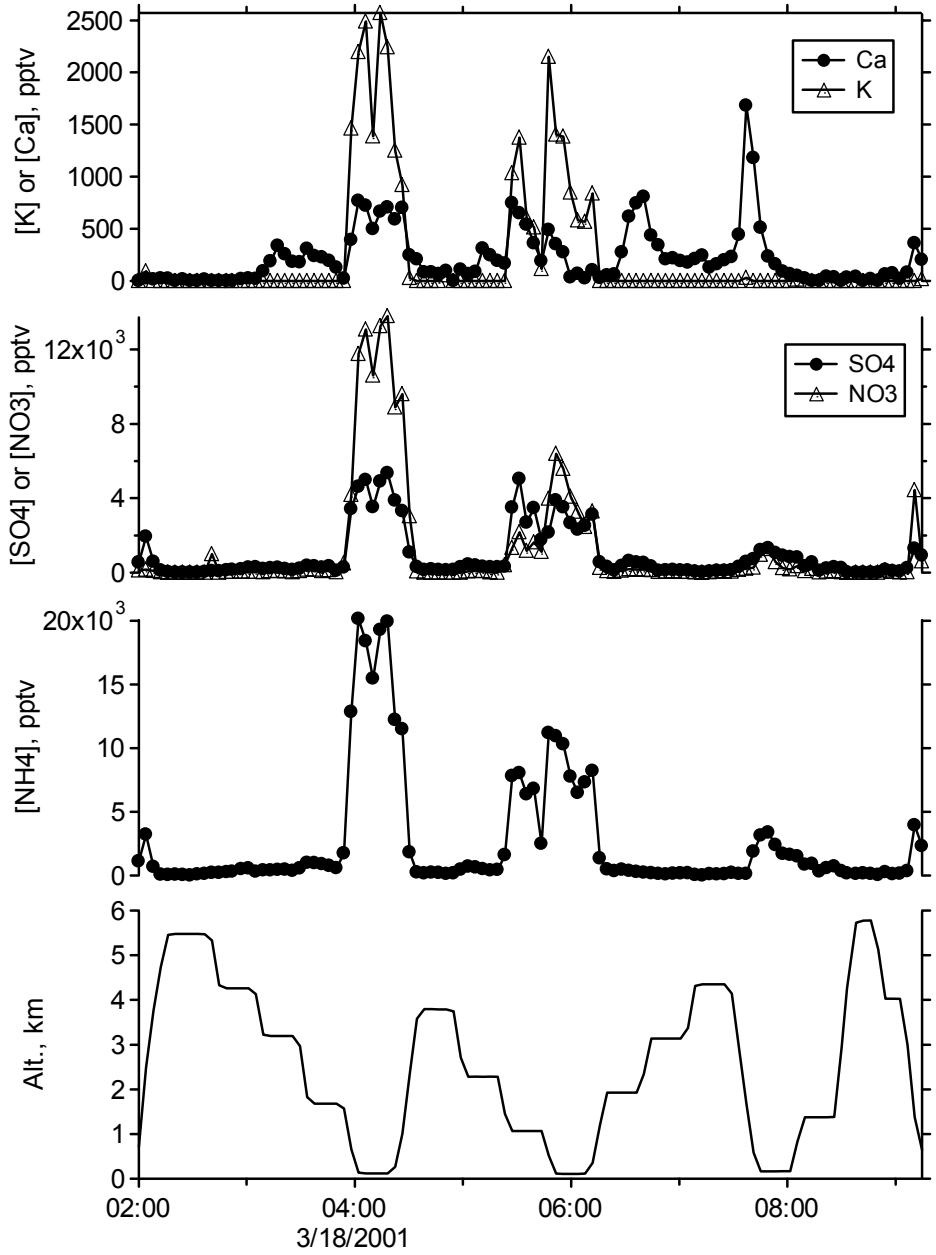

Figure 7. Correlation between aerosol Cl^- and Na^+. The solid lines represent the least squares fits. Data points in the shaded rectangular box were not used in the regression.

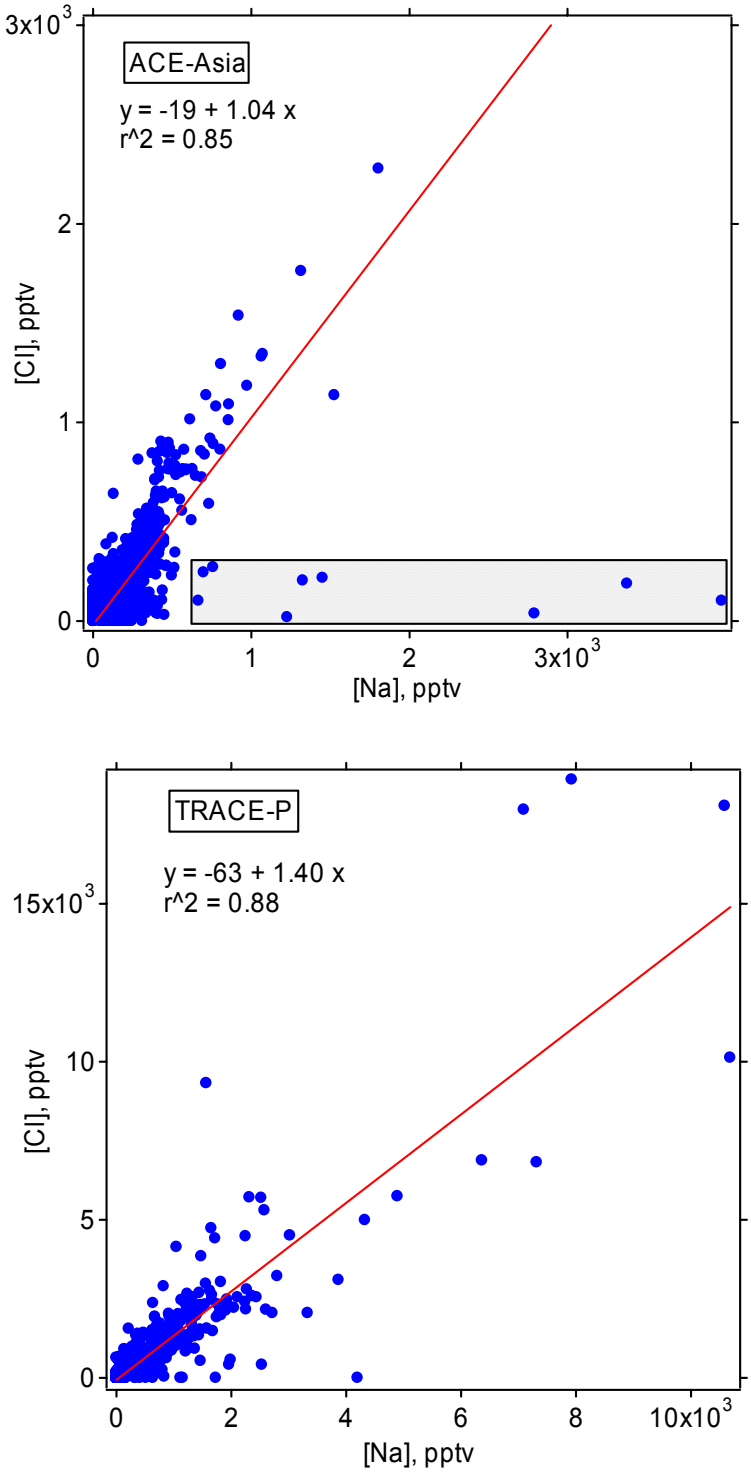

Figure 8. Scatter plot of Cl^- vs Na^+ observed on flight no. 14. The dashed line represents the sea water ratio of these two species (slope = 1.16). Data points are color-coded according to K^+ concentration.

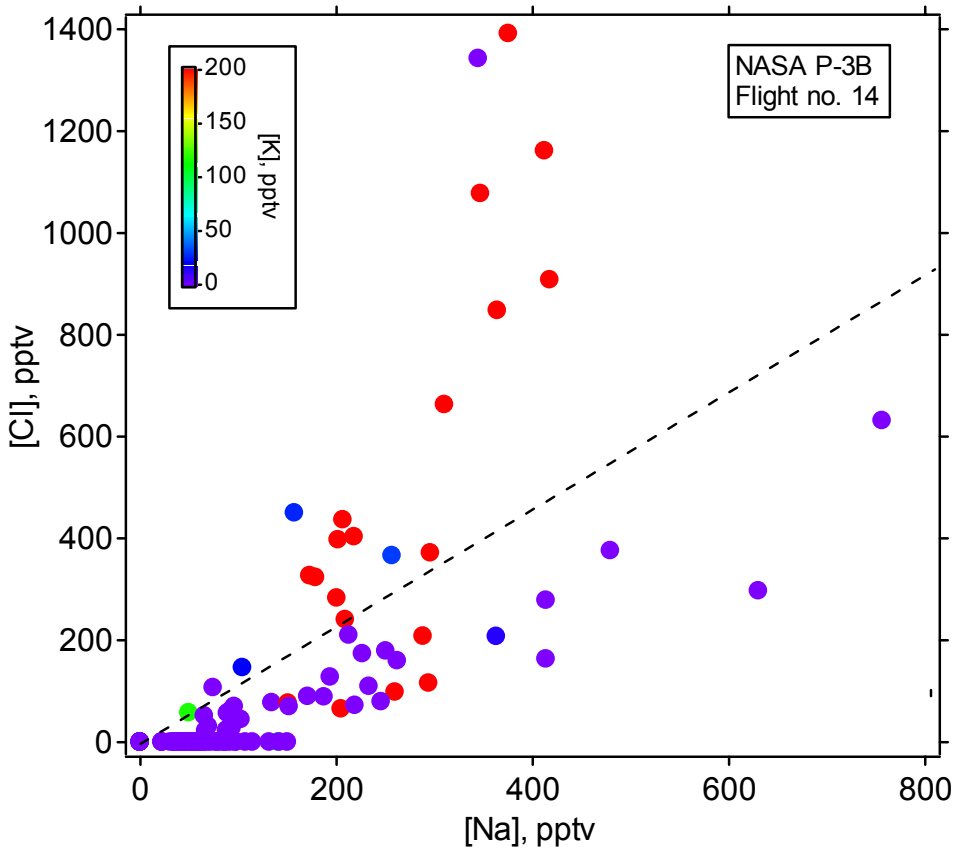

Figure 9. Correlation between Mg^{2+} and Ca^{2+}.

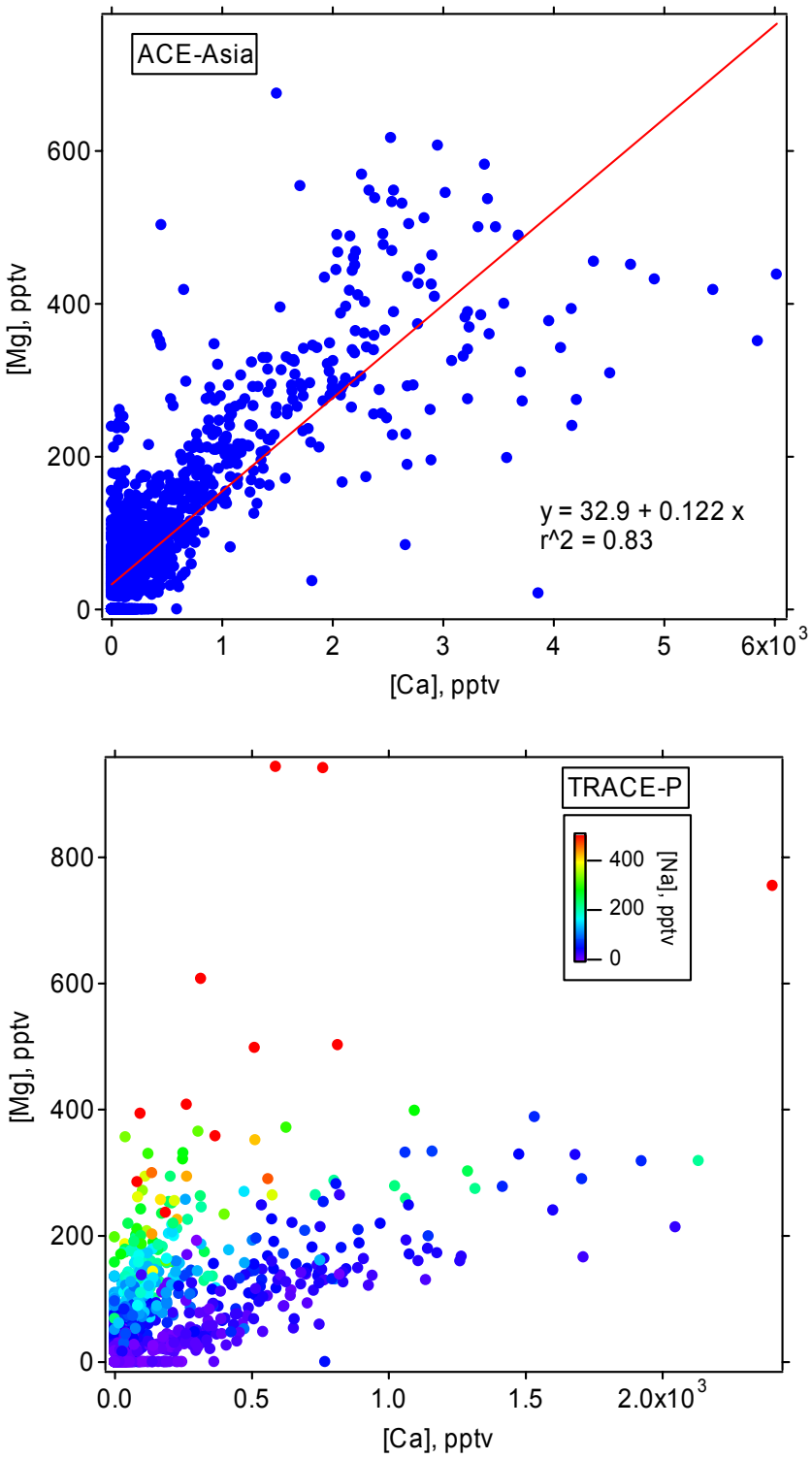

Figure 10. Correlation between NH_4^+ and the sum of NO_3^- and SO_4^{2-}. The solid line represents the best fit with data points (in red) showing a significant departure from the main group removed ($r^2 = 0.95$).

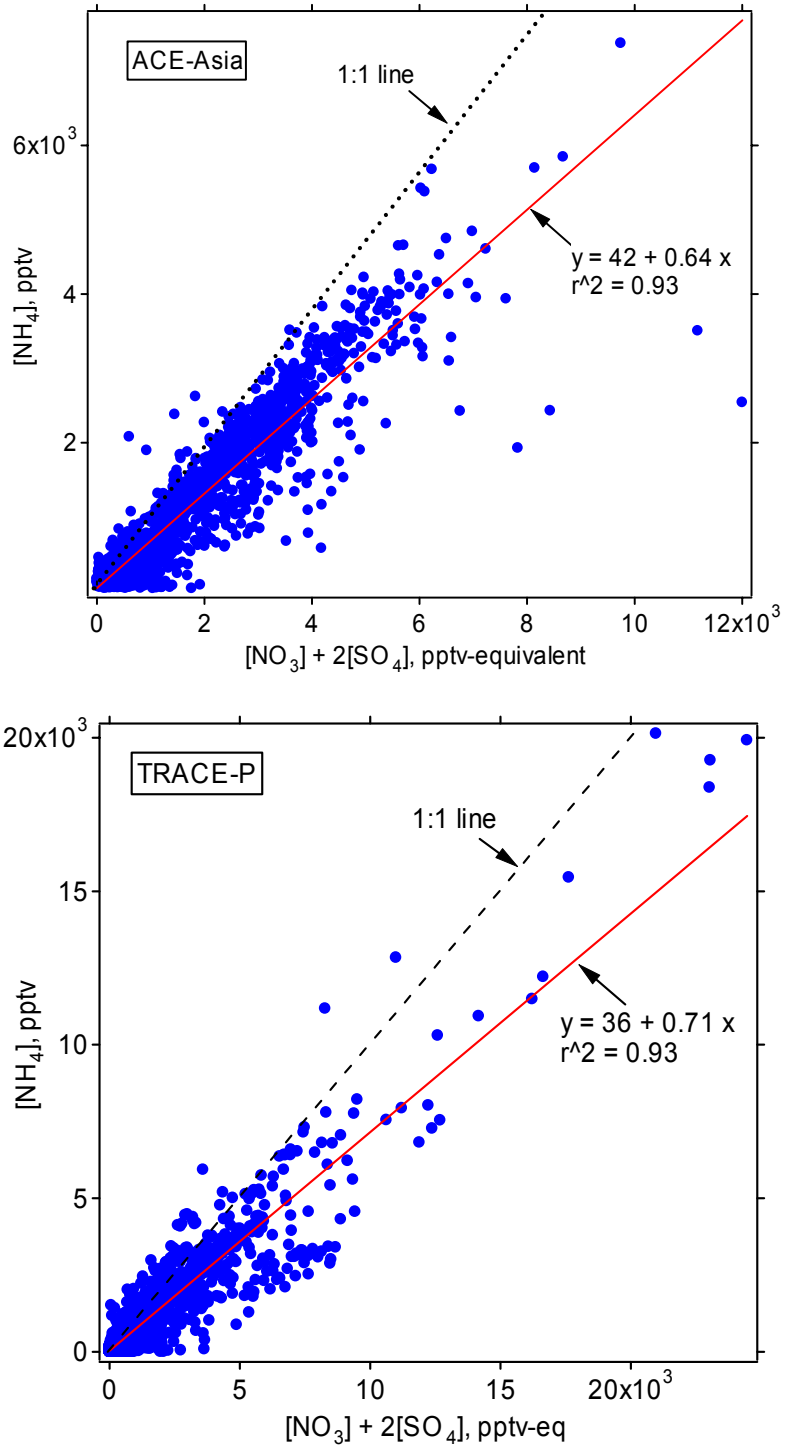

Figure 11. Altitude dependence of the ratio of NH_4^+ to the sum of NO_3^- and SO_4^{2-}. The solid curve represents the Lowess average, which approximates the median values. The dotted line is the slope of the best fit in the previous figure. Seventeen points with $[NH_4^+]/([NO_3^-]+2[SO_4^{2-}]$ ratio greater than 5, mostly in the altitude range 5 to 7 km, are not shown.

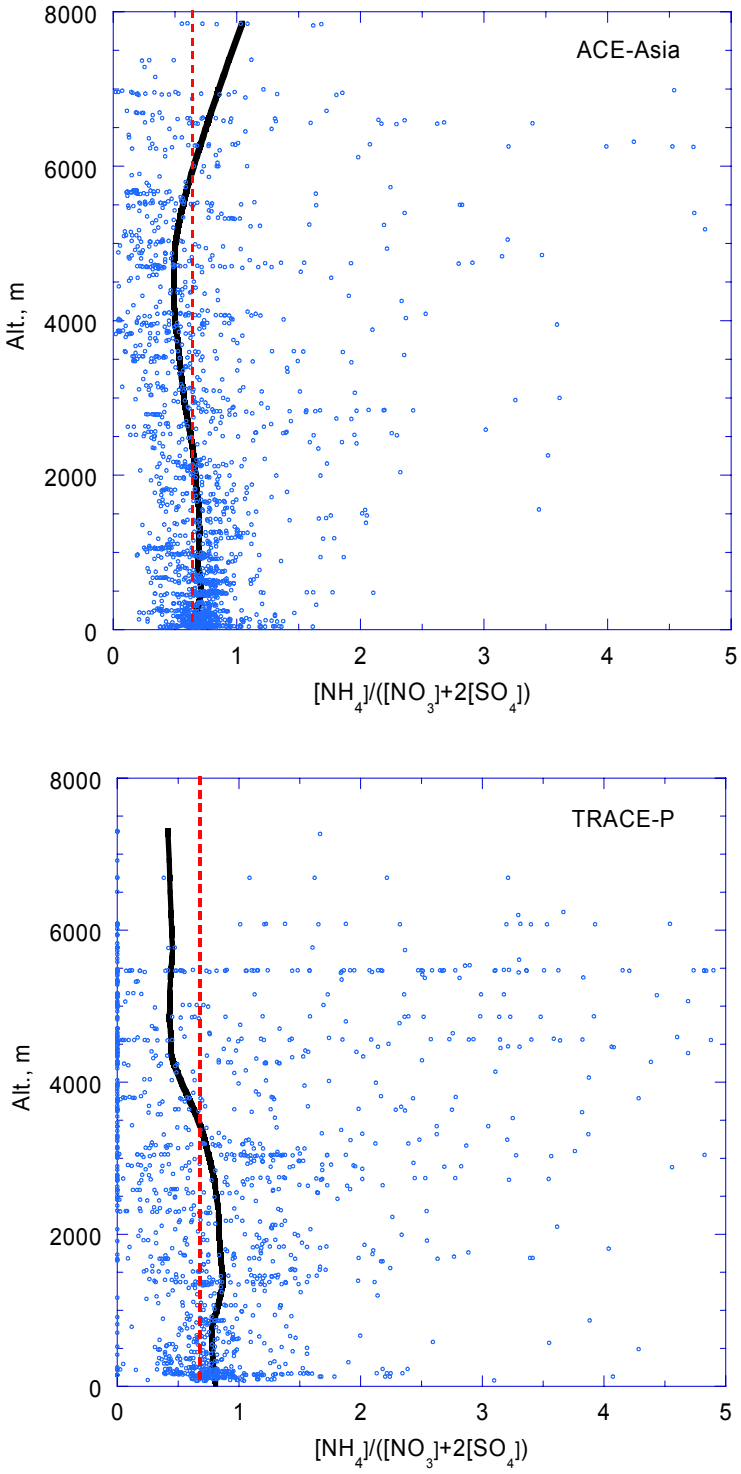

Figure 12. Ratio of $[NH_4^+]$ to $2[SO_4^{2-}]$ as a function of aerosol sulfate concentration observed during a P-3B volcano plume study (TRACE-P flight no. 17, 3/27/2001). Data are color coded to SO_2 concentration and size coded to altitude (less than 2 km if larger than the smallest point in the graph). The exponential fit of the data is limited to those associated with the Miyakejima volcanic plume using $[SO_2] > 2$ ppbv as a criterion. (SO_2 maximum was 17 ppbv, but clipped at 10 ppbv in the color scale for a better low range resolution.)

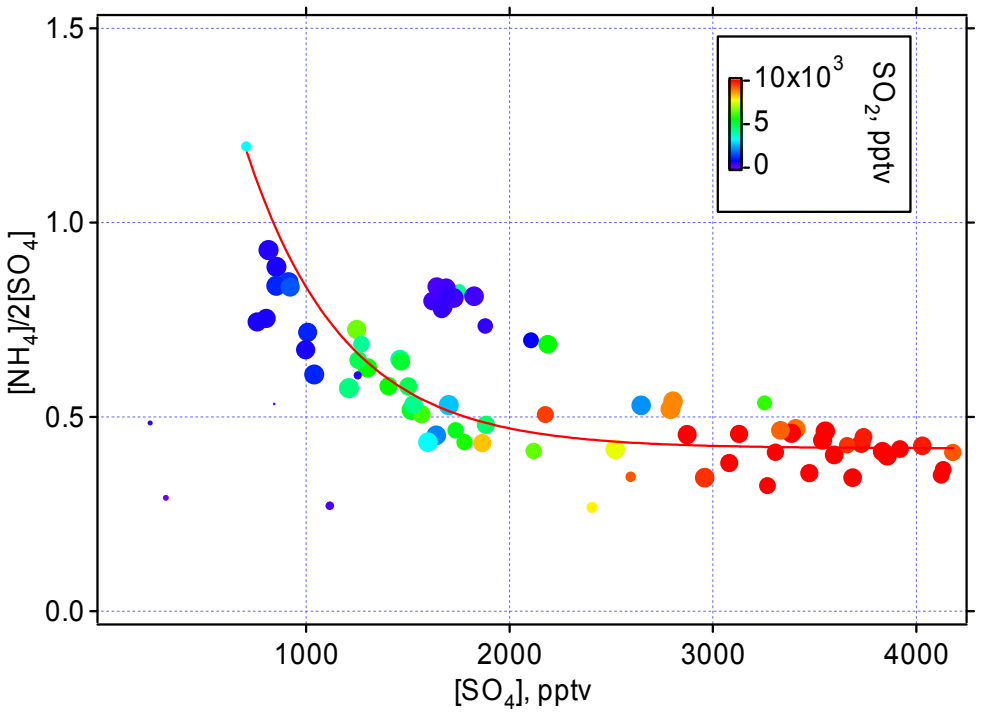

Figure 13. Relationship between aerosol SO_4^{2-} and SO_2 in the volcanic plume of Miyakejima. The solid line represents the best fit of the data for SO_2 > 2ppbv (r^2 = 0.80).

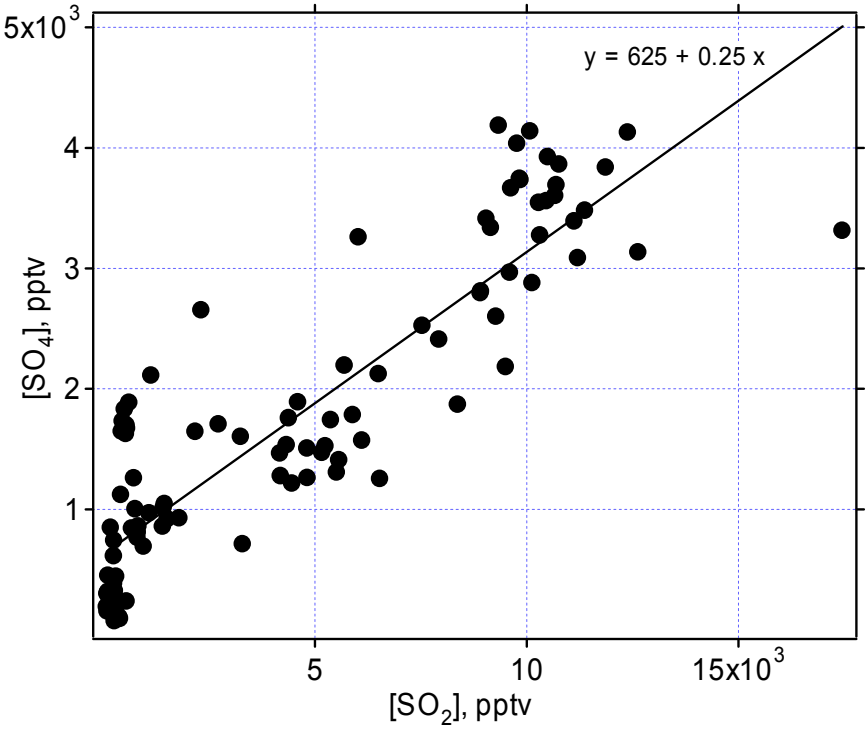

Figure 14. Charge balance of the measured aerosol ionic components during ACE-Asia. Top plot: color-coded to Ca concentration; the solid blue line is the least-square fit of data points. Bottom plot: without Ca^{2+}; the red data points are those identified in Figure 10 as having large $(NO_3^-+SO_4^{2-})/NH_4^+$ ratios.

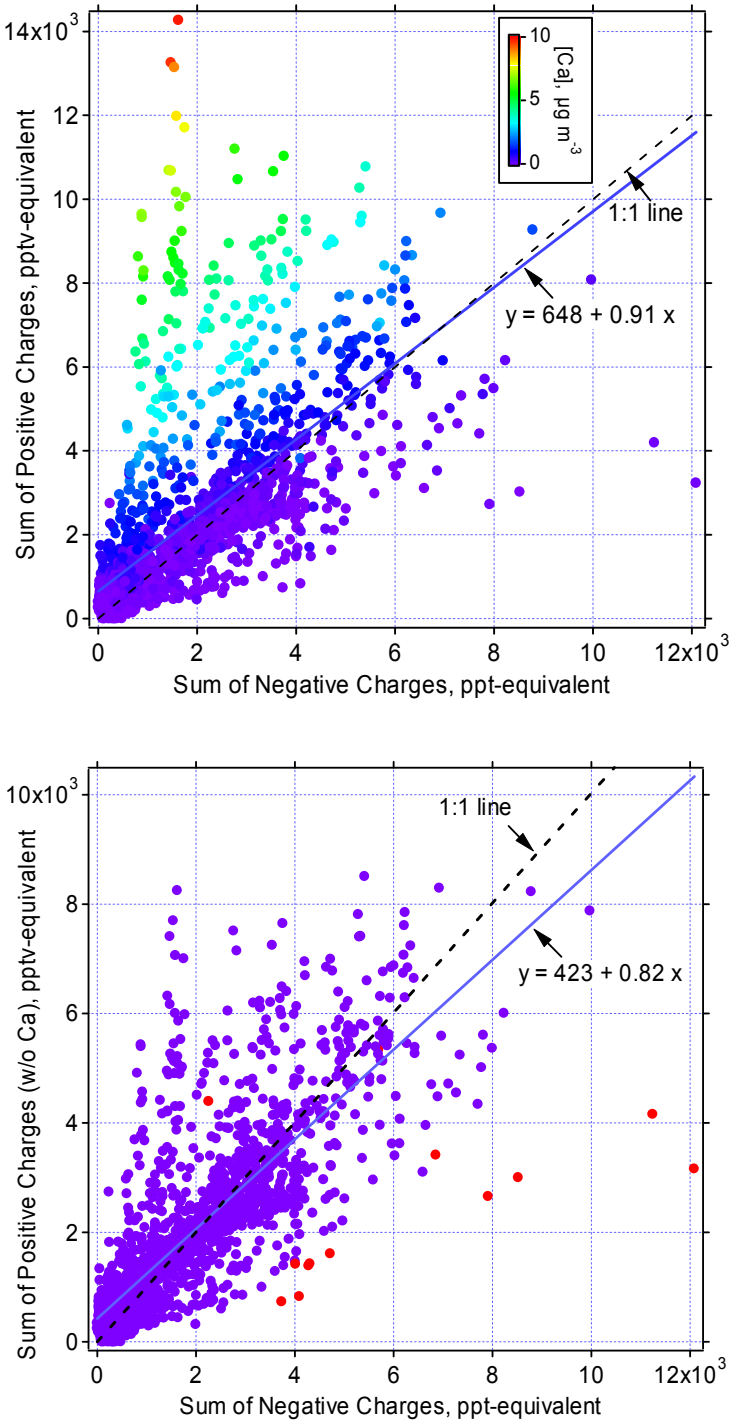

Figure 15. Charge balance of measured ions during TRACE-P. Top plot: Color coded to Ca^{2+} concentration. Bottom plot: color coded to SO_2 concentration; the two lines are the same as those in the top graph.

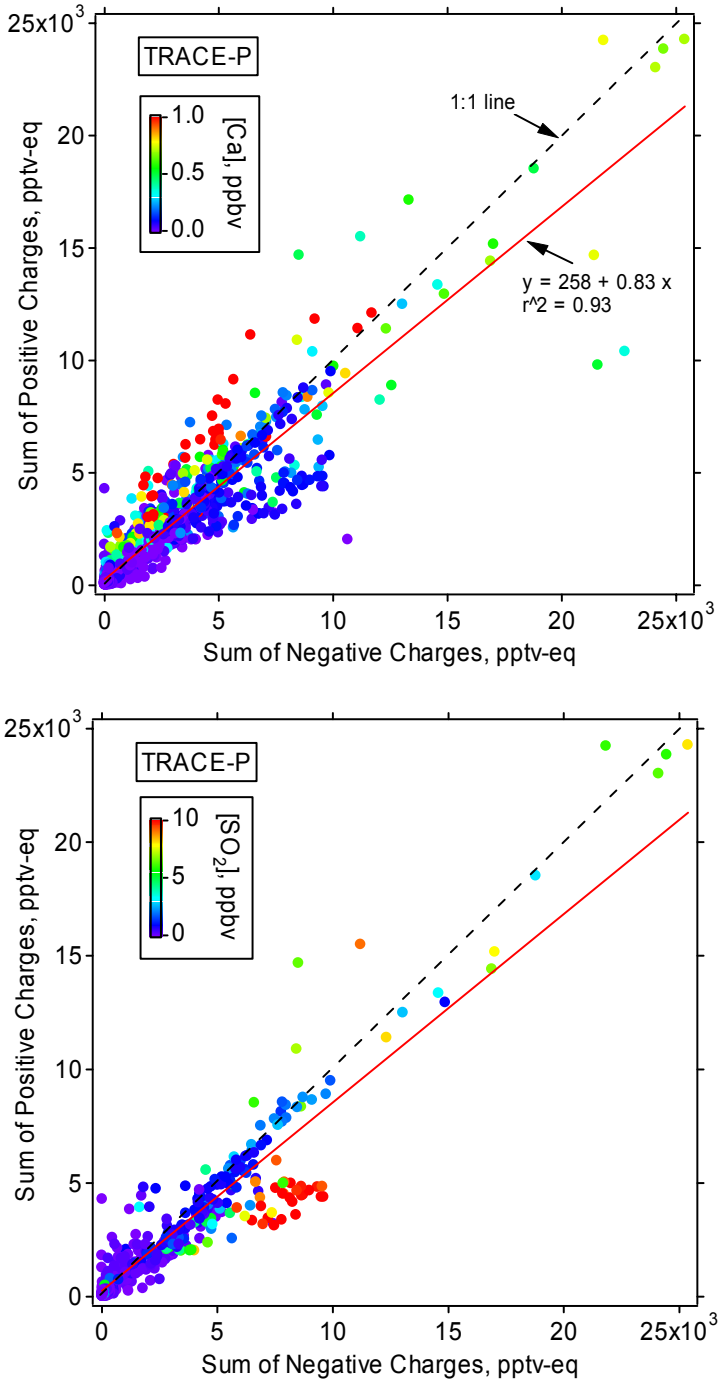

Figure 16. Charge imbalance of the measured aerosol ionic components as a function of total ion concentration. The solid line represents the best fit of the data and the upper panel shows the deviation of the imbalance from zero normalized to total ion concentration.

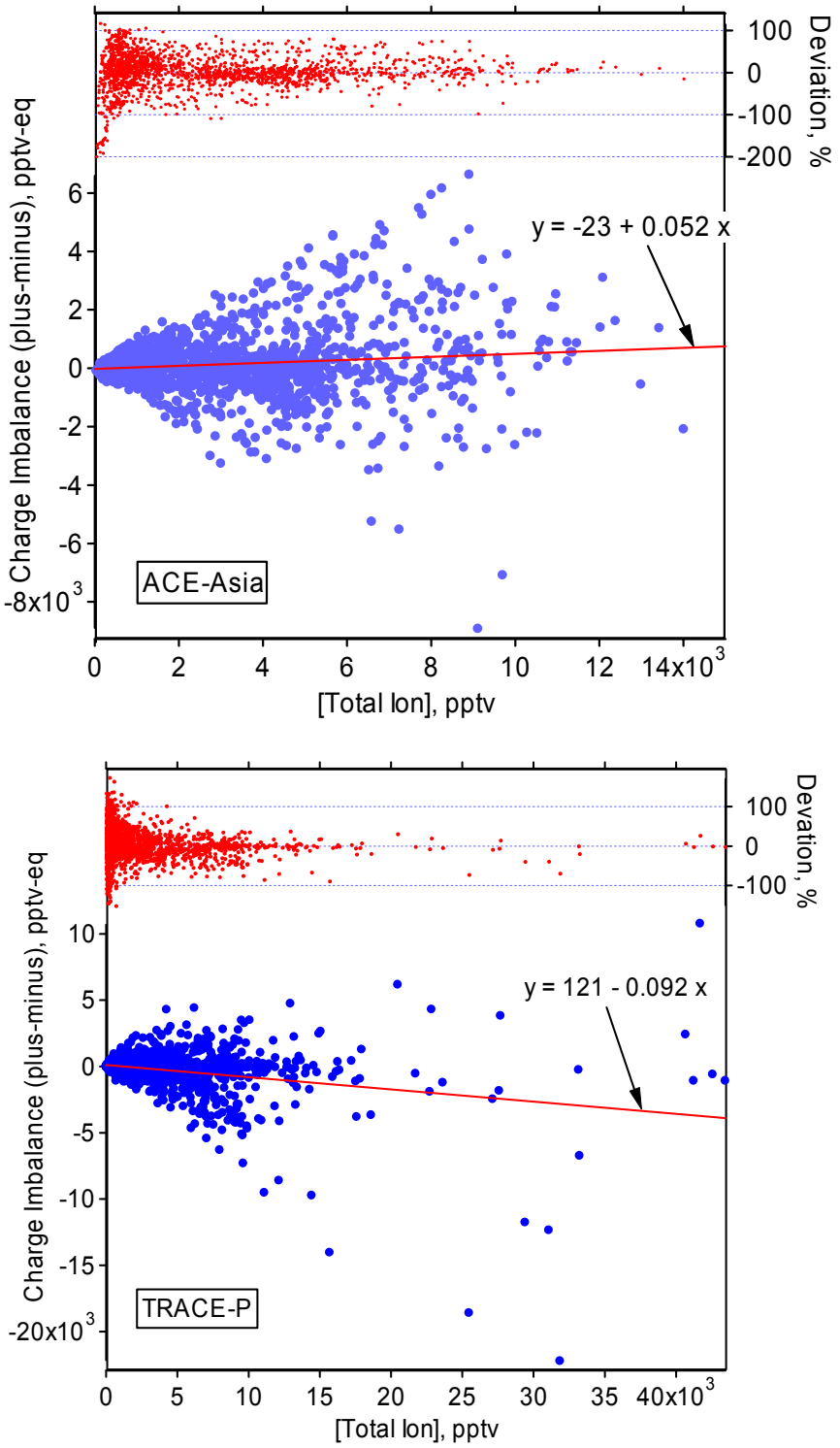

Figure 17. Ion imbalance as a function of altitude. Top plots: ACE-Asia. Bottom plot: TRACE-P. Points with a total ion concentration smaller than 500 pptv are shown in solid circles. The solid lines represent Lowess fits to the data.

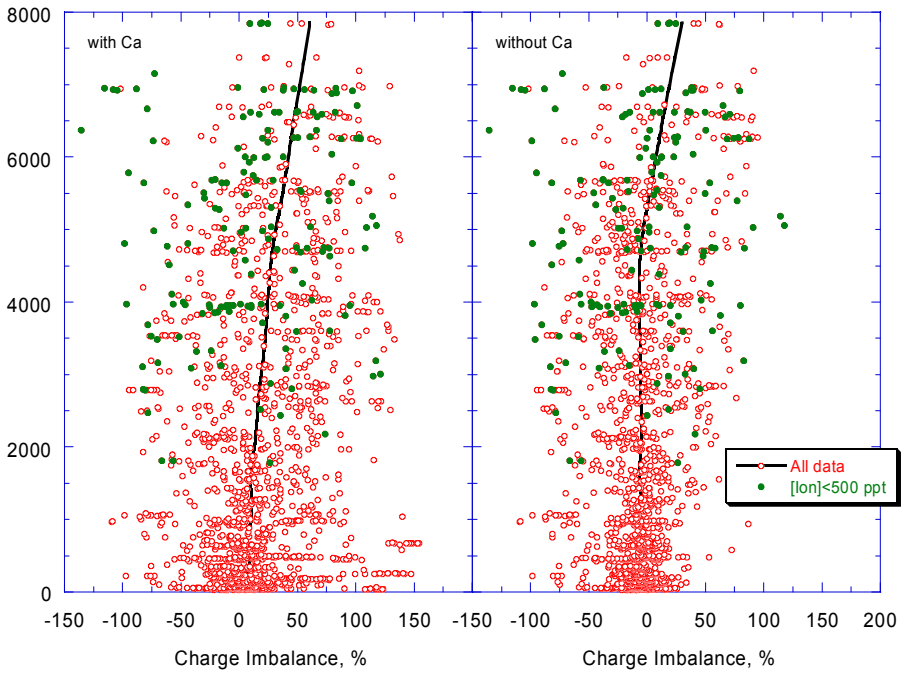

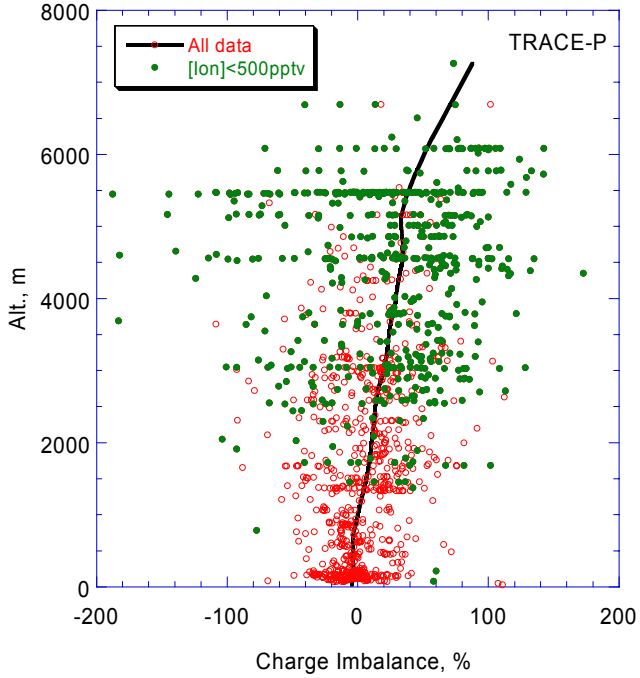

Figure 18. Correlation between the sum of ions (NO_3^-, SO_4^{2-}, NH_4^+, and K^+) and CO. Top: The group of points showing distinctly low ratios are treated separately; r^2 are 0.82 and 0.54, respectively. The dashed line is the eyeballed top edge of the data envelope. Bottom: The solid line is the best fit of the data without the group with [Ion] < 1 ppbv and [CO] > 250 ppbv. Dashed line is again the eyeballed top of the data envelop and the dotted line is the best fit line of the ACE-Asia data.

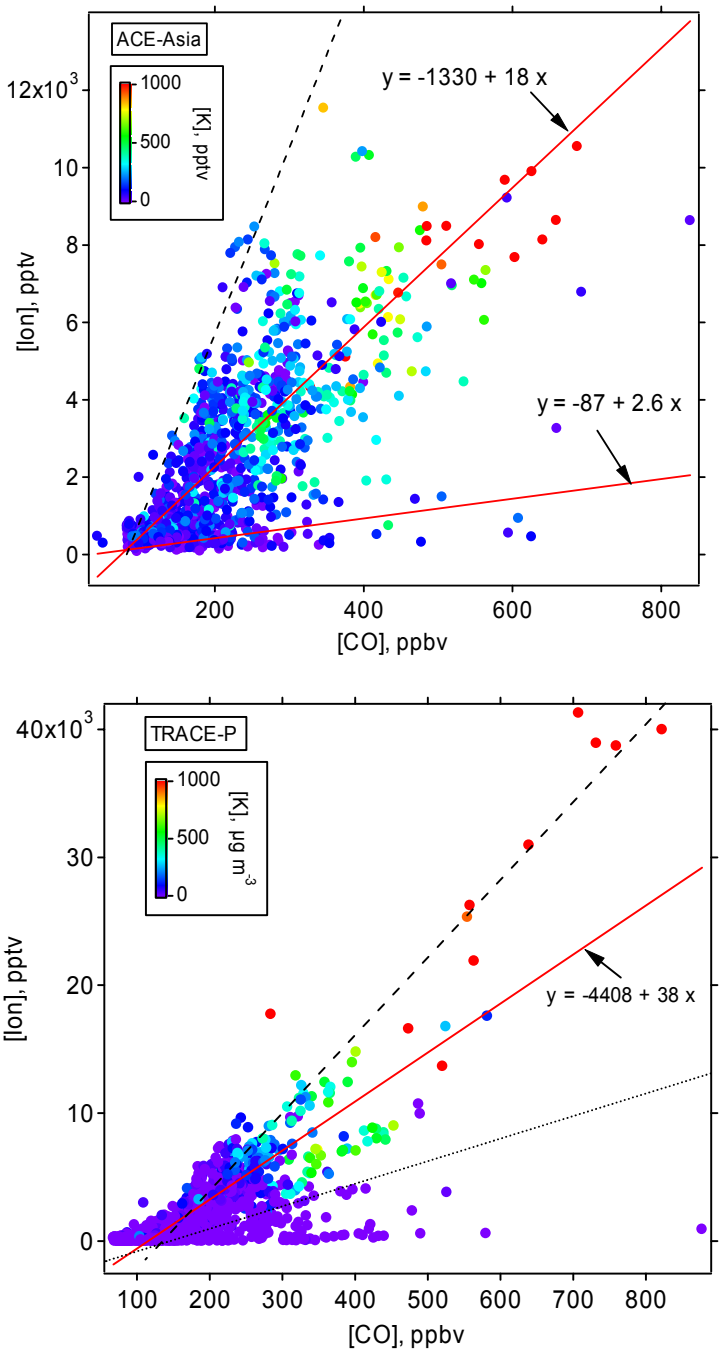

Figure 19. Contribution of Ca^{2+} to positive charges as a function of aerosol nitrate concentration.